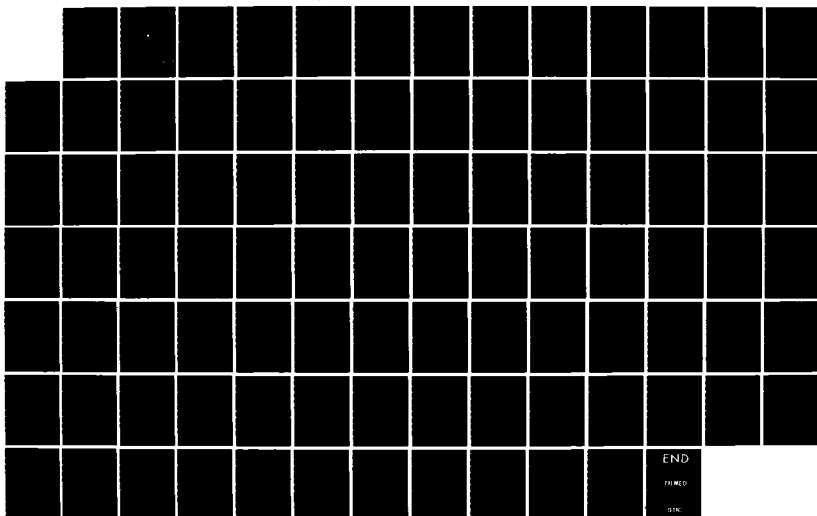AD-A154 250   LINEAR TIME-INVARIANT SPACE-VARIANT FILTERS AND THE WKB   1/1
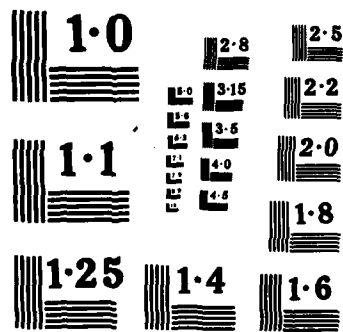   APPROXIMATION WIT..(U) NAVAL POSTGRADUATE SCHOOL
               MONTEREY CA J VOS DEC 84
UNCLASSIFIED   F/G 20/1   NL

NAVAL POSTGRADUATE SCHOOL
Monterey, California

THESIS

LINEAR TIME-INVARIANT SPACE-VARIANT FILTERS
AND THE WKB APPROXIMATION WITH APPLICATIONS
TO UNDERWATER ACOUSTIC SIGNAL PROCESSING

by

Jan Vos

December 1984

Thesis Advisor   Lawrence J. Ziomek

Approved for public release; distribution unlimited

DTIC
ELECTE
MAY 3 1 1985
S   D

D

85   5 28 076

REPORT DOCUMENTATION PAGE		READ INSTRUCTIONS BEFORE COMPLETING FORM
1. REPORT NUMBER	2. GOVT ACCESSION NO. A154230	3. RECIPIENT'S CATALOG NUMBER
4. TITLE (and Subtitle) Linear Time-invariant Space-variant Filters and the WKB Approximation with Applications to Underwater Acoustic Signal Processing		5. TYPE OF REPORT & PERIOD COVERED Master's Thesis December 1984
		6. PERFORMING ORG. REPORT NUMBER
7. AUTHOR(s) Jan Vos		8. CONTRACT OR GRANT NUMBER(s)
9. PERFORMING ORGANIZATION NAME AND ADDRESS Naval Postgraduate School Monterey, California 93943		10. PROGRAM ELEMENT, PROJECT, TASK AREA & WORK UNIT NUMBERS
11. CONTROLLING OFFICE NAME AND ADDRESS Naval Postgraduate School Monterey, California 93923		12. REPORT DATE December 1984
		13. NUMBER OF PAGES 92
14. MONITORING AGENCY NAME & ADDRESS(if different from Controlling Office)		15. SECURITY CLASS. (of this report) Unclassified
		15a. DECLASSIFICATION/DOWNGRADING SCHEDULE

16. DISTRIBUTION STATEMENT (of this Report)

Approved for public release; distribution unlimited

Accession For
NTIS GRA&I ☒
DTIC TAB ☐
Unannounced ☐
Justification

By
Distribution/
Availability Codes

Dist	Avail and/or Special
A-1	

17. DISTRIBUTION STATEMENT (of the abstract entered in Block 20, if different from Report)

18. SUPPLEMENTARY NOTES

19. KEY WORDS (Continue on reverse side if necessary and identify by block number)

Linear Time-invariant Space-variant Filters,
Wave Propagation in a Random Medium, The WKB Approximation,
Computer Simulated Output Electrical Signals, Three-dimensional
DFT Beamforming

20. ABSTRACT (Continue on reverse side if necessary and identify by block number)

    A computer simulation model is developed treating wave propagation in a random, inhomogeneous ocean as transmission through a linear time-invariant, space-variant random communication channel. The ocean volume is modelled by an index of refraction which is decomposed into a depth-dependent deterministic part and a depth-independent Gaussian zero-mean random part. Computer simulated output electrical signals were

DD FORM 1473 EDITION OF 1 NOV 65 IS OBSOLETE
1 JAN 73
S/N 0102-LF-014-6601

1

#20 - ABSTRACT - (CONTINUED)

generated that depend on the complex frequency spectrum of the transmitted electrical signal, the far-field beam pattern of the transmit array and the random transfer function of the ocean medium. Output was generated for different test cases. In all cases the transmit electrical signal was represented by a finite Fourier series and random cases were modelled by a random number generator. The computer simulated output electrical signals were then processed by a 3-D DFT beamformer and the results for the deterministic inhomogeneous and random inhomogeneous cases were compared to the homogeneous non-random case in order to study the effects of the medium on signal distortion and source localization.

Linear Time-Invariant Space-Variant Filters
and the WKB Approximation with Applications to
Underwater Acoustic Signal Processing

by

Jan Vos
Lieutenant, Royal Netherlands Navy
B.S., Delft University of Technology (Netherlands), 1981

Submitted in partial fulfillment of the
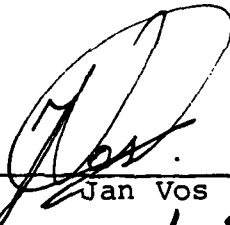requirements for the degree of

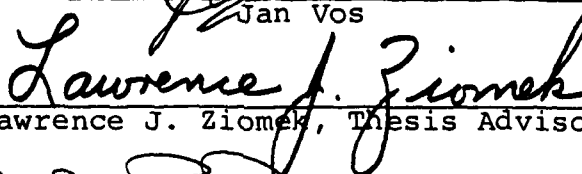MASTER OF SCIENCE IN ENGINEERING ACOUSTICS

from the

NAVAL POSTGRADUATE SCHOOL
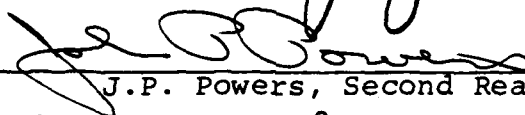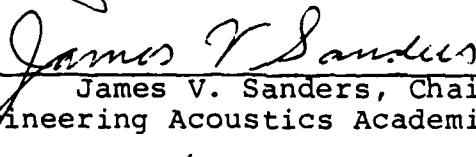December 1984

Author: _____
Jan Vos

_____
Lawrence J. Ziomek, Thesis Advisor

_____
J.P. Powers, Second Reader

_____
James V. Sanders, Chairman,
Engineering Acoustics Academic Committee

_____
John N. Dyer
Dean of Science and Engineering

3

ABSTRACT

A *mathematical* computer simulation model is developed treating *acoustic* wave propagation in a random, inhomogeneous ocean as transmission through a linear time-invariant, space-variant random communication channel. The ocean volume is modelled by an index of refraction which is decomposed into a depth-dependent deterministic part and a depth-independent Gaussian zero-mean random part. Computer simulated output electrical signals were generated that depend on the complex frequency spectrum of the transmitted electrical signal, the far-field beam pattern of the transmit array and the random transfer function of the ocean medium. Output was generated for different test cases. In all cases the transmit electrical signal was represented by a finite Fourier series and random cases were modelled by a random number generator. The computer simulated output electrical signals were then processed by a 3-D DFT beamformer and the results for the deterministic inhomogeneous and random inhomogeneous cases were compared to the homogeneous non-random case in order to study the effects of the medium on signal distortion and source localization.

4

TABLE OF CONTENTS

LIST OF TABLES

LIST OF FIGURES

ACKNOWLEDGMENT

The author expresses his sincere thanks to Professor L.J. Ziomek. His generous aid and encouragement have been of great support in completing this thesis.

I. INTRODUCTION

Based on the linearized acoustic wave equation for small
amplitude acoustic signals, sound propagation through the ocean
medium can be modelled as a signal passing through a linear
time-variant, space-variant random filter. The term "space-
variant" implies that the sound speed profile is a function
of position. The space variant property results in scatter
or angular spread due to refraction. If the filter is
"space-variant," then an isospeed medium is implied. As a
result, there will be no refraction, and hence, no scatter or
angular spread since the sound rays will be travelling in
straight lines. The term "time-variant" implies motion of,
for example, discrete point scatterers, the ocean surface,
and the transmit and receive arrays (apertures). The time-
variant property results in both Doppler spread and spread
in time delay.

By using a linear system's theory approach, different
propagation paths, such as direct paths, bottom reflected
paths and surface reflected paths, can be modelled as the
outputs from linear filters. Furthermore, different trans-
mit signals and transmit and receive far-field directivity
functions can easily be coupled to various transfer functions
of the random, inhomogeneous ocean medium in order to study
their effects on signal distortion and source localization
using various space-time signal processing algorithms.

Work based on this approach has been done by Laval [Refs. 5,6], Laval and Labasque [Ref. 7], Middleton [Refs. 8,9] and Ziomek [Ref. 1]. Middleton [Refs. 8,9] described propagation phenomena in a random inhomogeneous ocean with the use of space-time operators but did not concern himself directly with the derivation of random, time-variant, space-variant transfer functions.

Ziomek [Ref. 2] derived a time-invariant space-variant random transfer function of the ocean volume based on the WKB approximation. Ziomek [Ref. 3] also derived an equation for the random, output electrical signal at each element in a receive planar array of complex weighted point sources in terms of the frequency spectrum of the transmitted electrical signal, the transmit and receive arrays, and the random ocean medium transfer function.

The purpose of this thesis is to implement on a computer the equation for the output electrical signal as derived by Ziomek [Ref. 3]. This mathematical computer model simulates the effects of wave propagation through a random inhomogeneous ocean. The ocean volume is modelled by the transfer function derived in Ziomek [Ref. 2] and incorporates an index of refraction which is a function of depth. The index of refraction is decomposed into a depth-dependent deterministic component and a depth-independent zero mean Gaussian random component.

Section II is devoted to a theoretical description of the computer model. The notation and geometry of the computer

10

model are explained and the fundamental equations on which the computer model is based, are stated. Also, some additional constraints are made to allow for simpler implementation.

Section III describes the numerical techniques used and the resulting mathematical procedures which are implemented in the program. Furthermore, a brief outline of the computer program is given.

In Section IV a number of test cases are defined which were used to test the computer model. Computer simulated output electrical signals were generated for test cases incorporating deterministic homogeneous, deterministic inhomogeneous and random inhomogeneous medium models. The output signals were processed by a 3-D DFT beamformer and the results for the deterministic homogeneous case were used as the baseline case. Both deterministic and random inhomogeneous cases were compared to this baseline case in order to study the effects of the medium on signal distortion and source localization.

Note that the factor $1/c_n^2$ in equation (2.29) was moved in front and replaced by the factor $1/c_o^2$. This is possible because the differences in sound speed at the different transmitter elements are very small for all practical cases and the effect on the amplitude of $H(f,i,q)$ can be neglected. However, the dependence of the initial speed of sound on the index n of the transmit array will be taken into account in the evaluation of the phase terms as expressed by the different values of k_n in equation (3.1).

Using the definition of $H(f,i,q)$, the expression for the real output electrical signal at a receiver element with indices (i,q) becomes

$$y(t,i,q) = 2 \, \text{Re} \left\{ \sum_{k=1}^{KMAX} c_k H(kf_o,i,q) \exp(j2\pi k f_o t) \right\} \quad (3.2)$$

The computer program model first calculates $H(f,i,q)$ as given in equation (3.1). Then, with the use of $H(f,i,q)$, the output electrical signal is readily computed according to equation (3.2).

The ocean medium transfer function H_M is possibly random and therefore difficult to integrate numerically so a change in the order of integration in equation (3.1) is made to achieve a more suitable form for implementation:

25

III.   IMPLEMENTATION OF THE MODEL

The main task of the computer simulation model is to
compute and file the electrical output signal at all elements
of the receive planar array according to equation (2.29). The
model was implemented on an IBM system/370 mainframe computer
using FORTRAN. The program is computation intensive because
the evaluation of equation (2.29) involves a double integral
with nested summations. Therefore, much attention has been
given to program efficiency. This section discusses the
equations which were actually implemented and the overall logic
of the program.

A.   NUMERICAL METHODS

The model computes the real output electrical signal at
all receiver elements as given by equation (2.29). Note that
the double integral with respect to (w.r.t.) direction
cosines u_o and v_o behaves like a frequency response or trans-
fer function $H(f,i,q)$, which depends on the position of the
receiver elements as indicated by the indices (i.q). We define

$$H(f,i,q) \triangleq \frac{f^2}{c_o^2} \int_{-1}^{1} \int_{a_q}^{1} \sum_{n=-(N-1)/2}^{(N-1)/2} d_n \, H_M(k_n, v_o, n, q) \cdot$$

$$\exp[-jk_n v_o \Delta Y_{qn}] \exp[-jk_n(1-u_o^2-v_o^2)^{1/2}\Delta Z] \sum_{m=-(M-1)/2}^{(M-1)/2} c_m \exp[-jk_n \Delta X_{im} u_o] dv_o du_o$$

$$(3.1)$$

24

where f_o is the fundamental frequency $1/T_o$ and the DC term

is assumed to be zero. The complex Fourier series coefficients

c_k determine the amplitude and phase relations among the

different frequency components. The integral in equation

(2.22) now reduces to a summation and the expression for the

real output electrical signal at a receiver element with

indices i and q becomes:

$$y(t,i,q) \; = \; 2 \, Re \, \{ \sum_{k=1}^{KMAX} c_k (kf_o)^2 \int_{-1}^{1} \int_{a_q}^{1} \cdot$$

$$\sum_{n=-(N-1)/2}^{(N-1)/2} (d_n/c_n^2) H_M(k_n, v_o, n, q) \exp[-jk_n v_o \Delta Y_{qn}] \exp[-jk_n (1-u_o^2-v_o^2)^{1/2} \Delta z] \cdot$$

$$\sum_{m=-(M-1)/2}^{(M-1)/2} c_m \exp[-jk_n u_o \Delta X_{im}] dv_o \, du_o \exp[j2\pi kf_o t] \};$$
(2.29)

$$u_o^2 + v_o^2 \leq 1$$

23

generator. These restrictions make it possible to evaluate the transfer function with the closed form expressions given in equations (2.11), (2.16) and (2.19) for amplitude, deterministic phase component and random phase component of the transfer function, respectively. In the calculation of the random phase terms of the transfer function, a different random number was drawn for each combination of transmit element depth $y_o + nd_y$ and receive element depth $y_r + qd_y'$, thereby assuming that the random phase terms for the different transmission paths are uncorrelated.

3. Frequency Spectrum of the Transmitted Electrical Signal

The transmitted electrical signal was represented by a finite Fourier series with fundamental period T_o and maximum frequency f_{max} Hz:

$$f_{max} = KMAX \cdot \frac{1}{T_o} \qquad (2.27)$$

where KMAX denotes the total number of harmonics in the signal. This representation does not impose a severe restriction on the input signal, since every finite energy signal can be represented in the sense of a least mean-square error by a finite Fourier series. The expression for the frequency spectrum becomes:

$$X(f) = \sum_{k=1}^{KMAX} [c_k \delta(f - kf_o) + c_k^* \delta(f + kf_o)] \qquad (2.28)$$

Y-axis. Using Snell's law we find that at the turning point depth y_T:

$$c(y_T) = c_o/\sin(\beta_o) \qquad (2.24)$$

The relation between the angle β_o and v_o is given by:

$$v_o = \cos(\beta_o) \qquad (2.25)$$

Combining equations (2.24) and (2.25) into an inequality which has to be obeyed to avoid a turning point results in:

$$n(y) = \frac{c_o}{c(y)} > \sqrt{1 - v_o^2} \qquad (2.26)$$

and we conclude that obeying the inequality (2.23) also guarantees the absence of turning points.

2. Sound Speed Profile

The results presented in this thesis are based upon a sound speed profile which is assumed to have a constant gradient g and a random component of the index of refraction n_R which is not a function of depth. Note that the equations derived in Ziomek [Refs. 2,3] are more general and that the computer program described in this thesis can be easily modified to handle a more complex sound speed profile. For purpose of computer simulation, the random component of the index of refraction was assumed to be a zero mean, Gaussian random number with variance σ^2 and was modelled by a random number

21

receive arrays are used to couple an electrical signal to the medium and vice-versa.

The region of integration over direction cosine v_o is limited by a_q. This expresses the fact that the transfer function is not valid for direction cosine values v_o approaching 0 (close to a turning point). In most applications the limits of integration for both integrals can be further limited as shown in Section III.

B. CONSTRAINTS ON THE MODEL

In this section the inherent constraints on the model will be investigated. Also, some additional constraints will be made.

1. Geometrical Constraints

These constraints concern the transfer function which is only valid under the two following restrictions:

a. The assumption made in the derivation of the transfer function, in order to validate a binomial expansion was [Ref. 2]:

$$| [n^2(y) - 1]/v_o^2] | \quad < 1 \qquad (2.23)$$

Thus before using the computer model one should evaluate equation (2.23) for the chosen sound speed profile and array locations to make sure the inequality is obeyed.

b. Absence of turning points. The occurrence of turning points in a particular transmitter/receiver geometry depends on the initial direction of propagation, described by the angle β_o between the initial propagation vector and the

20

where

$$a_q = [|n_D^2(y_r + qd_y') - 1|]^{1/2}$$

$$\Delta Y_{qn} = y_r - y_o + qd_y' - nd_y$$

$$\Delta X_{im} = x_r - x_o + id_x' - nd_x$$

$$\Delta Z = z_r - z_o$$

$X(f)$: complex frequency spectrum of the transmitted electrical signal.

$c_n = c(y_o + nd_y)$; speed of sound at transmit element with index n.

$k_n = 2\pi f/c(y_o + nd_y)$; magnitude of initial propagation vector at transmit element with index n.

c_m, d_n: complex weights of the transmit array.

$H_M(f, f_y; y)$: Random time-invariant space-variant transfer function of the ocean medium. Note that H_M is a function of both indices q and n, i.e., it is a function of the y coordinate of the source location $y_o + nd_y$ and receiver location $y_r + qd_y'$. This can also be expressed by using the notation $H(k_n, v_o, n, q)$ expressing H_M as a function of wave number k_n, direction cosine v_o and indices n and q.

The above equations show how the medium transfer function is used in describing the acoustic field at a receiver location as a function of the acoustic field at a transmit location. The far-field directivity functions of transmit and

$$\theta_{MR} = -\frac{k_o}{v_o} n_R \int_{y_o}^{y} n_D(\zeta) d\zeta \qquad (2.18)$$

Substituting the equation of n_D for a constant gradient into equation (2.18) leads to:

$$\theta_{MR} = \frac{k_o}{v_o} \frac{c_o}{g} n_R \ln\{n_D(y)\} \qquad (2.19)$$

For a homogeneous medium, equations (2.16) and (2.19) become:

$$\theta_{MD} = 0 \qquad (2.20)$$

$$\theta_{MR} = -\frac{k_o}{v_o} n_R (y - y_o) \qquad (2.21)$$

Equations (2.11) through (2.13) for the amplitude and phase terms of the transfer function show that the medium has the effect of angle modulating the transmitted sound field, also referred to as scattering.

3. Output Electrical Signal

The output electrical signal at a receive location $(x_r+id'_x, y_r+qd'_y, z_r)$ is given by [Ref. 3]:

$$y(t, x_r+id'_x, y_r+qd'_y, z_r) = \int_{-\infty}^{\infty} X(f) \int_{-1}^{1} \int_{a_q}^{1} f^2 \cdot$$

$$\sum_{n=-(N-1)/2}^{(N-1)/2} (d_n/c_n^2) H_M(f, f_y; y) \exp\{-jk_n v_o \Delta Y_{qn}\} \exp\{-jk_n(1-u_o^2-v_o^2)^{1/2}\Delta z\} \cdot$$

$$\sum_{m=-(M-1)/2}^{(M-1)/2} c_m \exp\{-jk_n u_o \Delta X_{im}\} dv_o du_o \exp\{j2\pi ft\} df; \quad u_o^2+v_o^2 \le 1 \qquad (2.22)$$

18

$$\theta_{MR} = (-k_o^2/2\pi f_y) \int_{y_o}^{y} n_D(\zeta) n_R(\zeta) d\zeta \qquad (2.13)$$

This transfer function is valid in the absence of turning points and when the following inequality is obeyed:

$$|n^2(y) - 1|/v_o^2 < 1 \qquad (2.14)$$

In the case of a speed of sound profile with a constant gradient g, the deterministic component of the index of refraction becomes:

$$n_D(y) = c_o/(c_o + g(y-y_o)) \qquad (2.15)$$

Substitution into equation (2.12) results in

$$\theta_{MD} = \frac{k_o}{2v_o} \{ \frac{C_o}{g}[n_D(y) - 1] + y - y_o \} \qquad (2.16)$$

As far as the random phase term is concerned we will proceed by assuming that the random component of the index of refraction is not a function of depth and can be represented by a Gaussian, zero mean random variable with variance σ^2:

$$n_R(\zeta) = n_R = \sigma n_{NR} \qquad (2.17)$$

where n_R is $N(0,\sigma^2)$ and n_{NR}, which is the normalized random component of the index of refraction, is $N(0,1)$. When n_R is not a function of depth, equation (2.13) becomes:

17

from the center of the transmit array is, in general, not equal to k_o and is given by k_n:

$$k_n = 2\pi f/c(y_o + nd_y) \qquad (2.8)$$

One can also use spatial frequencies (in cycles/meter) to denote directions of propagation:

$$f_x = u_o/\lambda; \quad f_y = v_o/\lambda; \quad f_z = w_o/\lambda \qquad (2.9)$$

2. Transfer Function

The medium transfer function H_M is given by a function of frequency f, spatial frequency f_y and receiver depth y for a given source depth y_o [Ref. 2]:

$$H_M(f,f_y;y) = A_M(f,f_y;y)\exp\{j[\theta_{MD}(f,f_y;y)$$
$$+ \theta_{MR}(f,f_y;y)]\} \qquad (2.10)$$

where A_M is the amplitude term given by

$$A_M = (2\pi f_y)^{-1/2} = (k_o v_o)^{-1/2} \qquad (2.11)$$

and θ_{MD}, θ_{MR} are the deterministic and random phase terms, respectively:

$$\theta_{MD} = (-k_o^2/4\pi f_y) \int_{y_o}^{y} [n_D^2(\zeta) - 1]d\zeta \qquad (2.12)$$

16

The speed of sound in the medium is assumed to be only a function of depth and is given by $c(y)$. The reference speed of sound c_o is the speed of sound at the center of the transmit array, i.e., $c_o = c(y_o)$. The index of refraction $n(y)$ is a function of depth and is composed of a deterministic component and a random component:

$$n(y) = c_o/c(y) = n_D(y) + n_R(y) \qquad (2.3)$$

where n_D is the deterministic component and n_R is the random component of the index of refraction. The initial propagation vector will be denoted by $\underline{k}_n$, $k_o = 2\pi f/c_o$ is the magnitude of the initial propagation vector at depth $y = y_o$ (i.e., at the center of the transmit array). The components of the initial propagation vector along the x, y and z axes are described in terms of the direction cosines u_o, v_o and w_o:

$$k_x = k_o u_o \qquad (2.4)$$

$$k_y = k_o v_o \qquad (2.5)$$

$$k_z = k_o w_o \qquad (2.6)$$

and

$$w_o^2 = 1 - u_o^2 - v_o^2 \qquad (2.7)$$

Note that the magnitude of the initial propagation vector at the transmit elements which are located at a depth nd_y meters

15

describes the wave propagation between a transmit planar array and a receive planar array whose centers are located at (x_o, y_o, z_o) and (x_r, y_r, z_r), respectively. The x, y and z axes describe cross range, depth and range, respectively. The transmit array, which is a parallel to the XY plane, consists of $M \times N$ complex weighted point sources, where M and N are odd. The sources are equally spaced in the X- and Y-directions with spacings of d_x and d_y meters, respectively. Note that in general $d_x \neq d_y$. The complex weights are assumed to be separable and given by

$$c_m = a_m \exp\{j\theta_m\} \qquad (2.1)$$

for the weighting in the X-direction and by

$$d_n = b_n \exp\{j\phi_n\} \qquad (2.2)$$

for the weighting in the Y-direction. The combined weight factor for each transmit element is $c_m d_n$, where m and n are the indices describing the transmit element at position $(x_o + md_x, y_o + nd_y, z_o)$. The complex weights are used for amplitude shading and beamsteering of the transmit beam pattern. The receive planar array, which is also parallel to the XY plane, consists of $M' \times N'$ elements, where M' and N' are odd. The sources are equally spaced in the X- and Y-directions with spacings of d'_x and d'_y meters, respectively, where in general $d'_x \neq d'_y$. The position of a receiver element with indices (i,q) is given by $(x_r + id'_x, y_r + qd'_y, z_r)$.

14
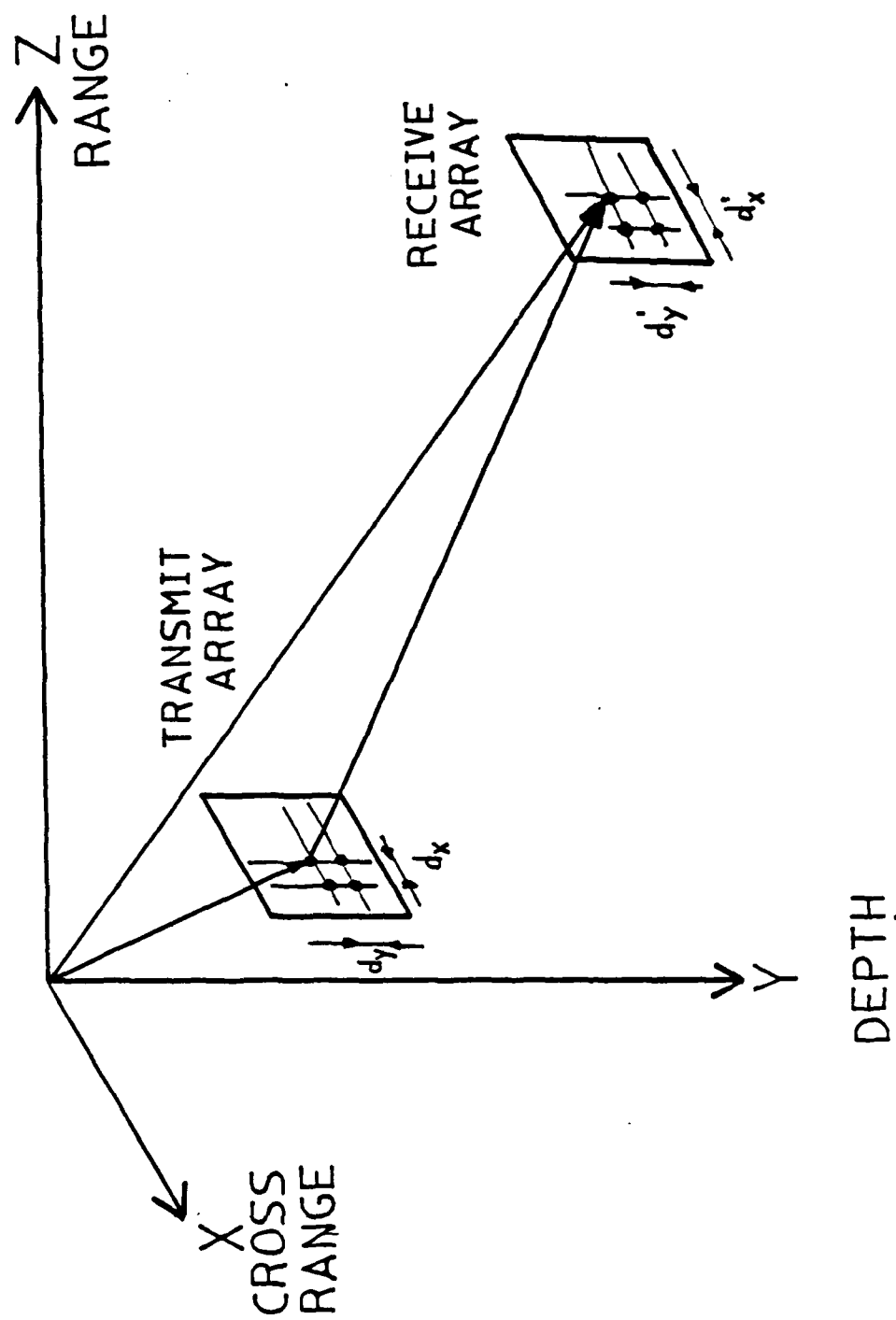
Fig. 1   Model Geometry

II. THEORY ON THE COMPUTER SIMULATION MODEL

A. MODEL DESCRIPTION

The mathematical computer model calculates the output
electrical signal at each element of a receive planar array
of point sources in terms of the complex frequency spectrum
of the transmitted electrical signal, the transmit and receive
arrays, and the random ocean medium transfer function. The
theory for the model is based on time-variant, space-variant
random filters as discussed in Ziomek [Ref. 1]. Ziomek [Ref.
2] derived a time-invariant space-variant transfer function
for a random ocean volume where the index of refraction, which
is composed of a deterministic and a random component, is a
function of depth. This transfer function is based on the
WKB approximation, which is a solution to the wave equation
when the index of refraction is a function of depth. Further-
more, Ziomek [Ref. 3] derived an equation for the random
output electrical signals appearing at each element in a
receive planar array of complex weighted point sources in
terms of the frequency spectrum of the transmitted electrical
signal, the transmit and receive arrays, and the random ocean
transfer function. The computer model combines and implements
the equations derived by Ziomek [Refs. 2,3] for the transfer
function and the output electrical signals.

1. Geometry of the Model

Figure 1 shows the geometry of the communication
channel as simulated by the computer model. The model

12

$$H(f,i,q) = \frac{f^2}{c_o^2 \, a_q} \int_{-1}^{1} \sum_{n=-(N-1)/2}^{(N-1)/2} d_n H_M(k_n, v_o, n, q) \exp[-jk_n v_o \Delta Y_{qn}] \cdot$$

$$\int_{-1}^{1} \sum_{m=-(M-1)/2}^{(M-1)/2} c_m \exp[-jk_n u_o \Delta X_{im}] \exp[-jk_n(1-u_o^2-v_o^2)^{1/2}\Delta Z] du_o \, dv_o \quad (3.3)$$

In order to improve efficiency, we concentrate first on the inner integral w.r.t. u_o, which we rewrite as

$$\int_{-1}^{1} S_X(f, u_o) \exp\{-k_n[u_o \Delta X_i + (1-u_o^2-v_o^2)^{1/2}\Delta Z]\} du_o \quad (3.4)$$

where:

$$\Delta X_i = x_r - x_o + id_x'$$

Note that

$$S_X(f, u_o) = \sum_{m=-(M-1)/2}^{(M-1)/2} c_m \exp[jk_n u_o m d_x] \quad (3.5)$$

is the transmit far-field directivity function of a line array consisting of equally spaced point-sources as a function of direction cosine u_o and frequency f. Now equation (3.3) reduces to:

$$H(f,i,q) = \frac{f^2}{c_o^2 \, a_q} \int_{-1}^{1} \sum_{n=-(N-1)/2}^{(N-1)/2} d_n H_M(k_n, v_o, n, q) \exp[-jk_n v_o \Delta Y_{qn}] \cdot$$

$$\int_{-1}^{1} S_X(f, u_o) \exp\{-jk_n[u_o \Delta X_i + (1-u_o^2-v_o^2)^{1/2}\Delta Z]\} du_o \, dv_o \quad (3.6)$$

26

In the case of simple amplitude weighting in the x-direction such as rectangular, triangular or Hamming weighting, we can obtain closed form expressions for $S_X(f,u_o)$. This improves program efficiency. For example, in the case of rectangular amplitude weighting

$$S_X(f,u_o) = \frac{\sin[k_n(u_o - u_b)Md_x/2]}{\sin[k_n(u_o - u_b)d_x/2]} \qquad (3.7)$$

where u_b is the direction cosine value to which the transmit far-field beam pattern is steered.

Before presenting more details on how $H(f,i,q)$ is calculated, a brief overview on numerical and analytical integration techniques which were used is given.

1. Integration Techniques

   a. Method of Stationary Phase

      This method approximates an integral of the form

$$I = \int_a^b S(z) \exp[jg(z)]dz \qquad (3.8)$$

where $g(z)$ is a rapidly varying phase term compared to the slowly varying amplitude term $S(z)$. Officer [Ref. 10] shows that this integral can be approximated by using the fact that the main contribution exists at the stationary point z_{sp} which is defined by

$$\frac{dg(Z_{sp})}{dz} = 0 \qquad (3.9)$$

27

The limits of the integral may be extended to infinity because only the region around the stationary point contributes to the integral. Assume that around the stationary point, z is given by

$$z = z_{sp} + \zeta \qquad (3.10)$$

The approximation of the integral is then given by

$$I = S(z_{sp}) \sqrt{2\pi / |g''(z_{sp})|} \exp\{j [g(z_{sp}) \pm \tfrac{\pi}{4}]\} \qquad (3.11)$$

under the condition:

$$\frac{|\zeta g'''(z_{sp})|}{|3g''(z_{sp})|} \ll 1 \qquad (3.12)$$

where the sign in the phase term of equation (3.11) equals the sign of the second derivative $g''(z_{sp})$.

b. Numerical Integration Using Newton-Cote's Formulas

This standard technique [Ref. 11] is the method used by the program to perform a numerical integration over a subinterval of the total region of integration. Subintervals can be defined by dividing the total region of integration into equal parts or by a scheme as described in the next section. Each subinterval is integrated by evaluating the Simpson's rule estimate:

$$S = \frac{h}{3}(s_o + 2s_1 + 4s_2 + 2s_3 + 4s_4 + \ldots + 2s_{n-1} + s_n)$$

$$(3.13)$$

28

where $s_o, \ldots, s_n$ denote values of the integrand evaluated at different points of the subinterval, and the distance between these points is given by the step size h. The original step size h is equal to half the size of the subinterval to be integrated. The step size is then halved to obtain a more accurate estimate which takes more points into account. This is repeated until a tolerance criterion is met. Using successive Simpson's rule estimates, one can do a Richardson's extrapolation [Ref. 12]. This extrapolation uses the last two estimates by Simpson's rule, S_2 and S_1, where S_2 uses half the step size of S_1. Both estimates have a global error of order h^4. The extrapolated value becomes:

$$\text{Extrapolated value } = S_2 + (S_2 - S_1)/15 \qquad (3.14)$$

with an error of order h^6. If two successive extrapolated values are within tolerance, the last extrapolated value is taken as the value of the integral for that subinterval. This scheme creates a semi-adaptive integration procedure because different subintervals can require different step sizes. It could be further enhanced but would then require more overhead. Another possibility would be the use of a Gaussian quadrature rule which needs less function evaluations for the same order of error but has the disadvantage that the points are not identically spaced and the scheme cannot be made adaptive in a computation efficient manner.

c. Numerical Integration Using the Euler Summation

A problem in evaluating an integral like equation (3.4) is convergence. The real and imaginary parts of the integrand of equation (3.4) are oscillatory. Successive positive and negative contributions tend to cancel, but each contribution itself is not negligible and the integral behaves oscillatory as a function of its limits of integration. Therefore, one has to integrate over a relatively large region to obtain convergence. This is in conflict with the desired computational efficiency.

Squire [Ref. 13: pp. 172-173] describes an integration procedure for oscillatory integrands which splits the range of integration into parts using the zero crossings of the integrand as points of separation. The individual subintervals can be evaluated with the use of standard methods (as described in III.A.1.b) and summed to form the value of the integral. A technique like the Euler summation [Ref. 13: pp. 172-173] can be used to improve convergence of this summation. The Euler summation obtains from an original sequence

$$a_1, a_2, a_3, \ldots, a_n$$

a second sequence

$$b_1 = a_2 + a_1, \quad b_2 = b_3 + a_2, \quad \ldots, \quad b_k = a_k + a_k + 1$$

and a third sequence

$$c_1 = b_2 + b_1, \quad c_2 = b_3 + b_2, \quad \ldots, \quad c_k = b_{k+1} + b_k$$

and so on. It can be shown that the sum of

$$\frac{1}{2} a_1 + \frac{1}{4} b_1 + \frac{1}{8} c_1 + \ldots + \frac{1}{2^m} m_1$$

is the same as the sum of the original sequence. Convergence however is much improved which cuts down on the number of subintervals to be integrated and improves efficiency.

This method works well on integrals where successive contributions from subintervals to the integral are of decreasing magnitude and of alternating sign as illustrated in Figure 2. To use this method it must be possible to solve for the zero crossings of the integrand, which generally requires a closed form expression to solve for the roots of the integrand.

2. Application of Integration Methods

The methods introduced in the previous section are used to define a procedure to calculate $H(f,i,q)$. First, the integration w.r.t. direction cosine u_o is considered, which is given by

$$\int_{-1}^{1} S_x(f,u_o) \exp\{-jk_n [u_o \Delta X_i + (1-u_o^2-v_o^2)^{1/2} \Delta z]\} du_o \qquad (3.4)$$

Both the method of stationary phase and the numerical method (Sections III.A.1.b and III.A.1.c) using the Euler summation are implemented. To apply the method of stationary

31
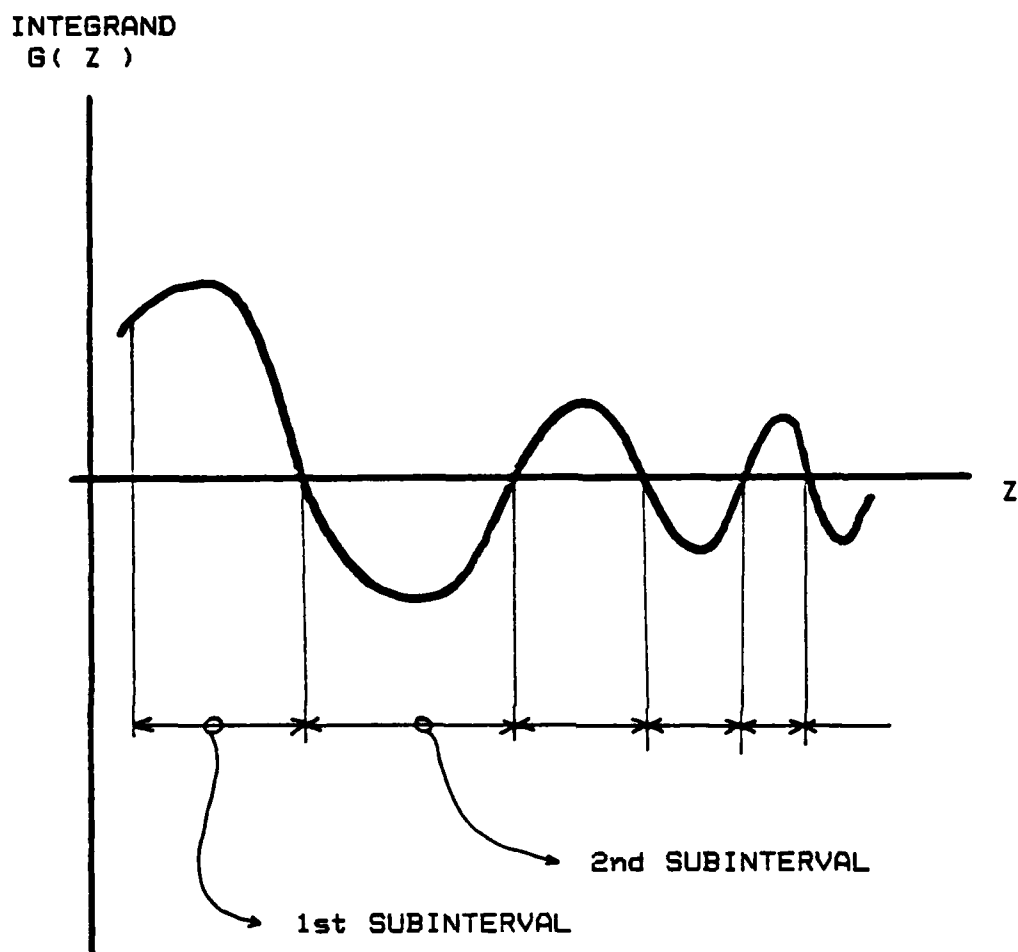
Fig. 2   Oscillatory Integrand Showing Decreasing
          Contributions to the Integral

phase we define in accordance with equation (3.8)

$$g(u_o) = -k_n[\Delta X_i u_o + (1 - u_o^2 - v_o^2)^{1/2} \Delta Z] \qquad (3.15)$$

The amplitude term $S_x(f, u_o)$ is the directivity function which is indeed slowly varying w.r.t. $g(u_o)$. We find the stationary point UOSP by setting $g'(UOSP)$ equal to zero:

$$g'(UOSP) = -k_n \Delta X_i + k_n \Delta Z (1 - u_o^2 - v_o^2)^{-1/2} u_o = 0 \qquad (3.16)$$

leading to

$$UOSP = \frac{\Delta X_i}{\Delta Z} \left(\frac{1 - v_o^2}{1 + (\Delta X_i / \Delta Z)^2} \right)^{1/2} \qquad (3.17)$$

For the values of the second and third derivatives one finds

$$g''(u_o) = k_n \Delta Z (1 - u_o^2 - v_o^2)^{-3/2} (1 - v_o^2) \qquad (3.18)$$

$$g'''(u_o) = 3k_n \Delta Z u_o (1 - u_o^2 - v_o^2)^{-5/2} (1 - v_o^2) \qquad (3.19)$$

We now form the ratio of the third and second derivatives at u_o equal to the stationary point UOSP:

$$\frac{g'''(UOSP)}{g''(UOSP)} = 3\Delta X_i (1 - v_o^2)^{-1/2} \frac{(\Delta X_i^2 + \Delta Z^2)^{1/2}}{\Delta Z^2} \qquad (3.20)$$

The condition in equation (3.12) becomes

$$\left| \zeta \left(\frac{\Delta X_i}{\Delta Z} \right) \sqrt{\frac{1 + (\Delta X_i / \Delta Z)^2}{1 - v_o^2}} \right| \ll 1 \qquad (3.21)$$

from which we conclude that the above condition is obeyed only when $\Delta Z \gg \Delta X_i$, which means that the method is only valid for relatively small cross ranges $x_r - x_o$ since $\Delta X_i = x_r - x_o + i\, d_x'$.

The program implements the following procedure to compute the magnitude and phase of the integral w.r.t. u_o [see equation (3.4)], denoted by IWRTUO.

1) Calculate the stationary point UOSP

$$\text{UOSP} = \frac{\Delta X_i}{\Delta Z} \sqrt{\frac{1 - v_o^2}{1 + (\Delta X_i / \Delta Z)^2}} \qquad (3.17)$$

2) Calculate the value of the second derivative DRV2ND at the stationary point:

$$\text{DRV2ND} = k_o \Delta Z (1 - \text{UOSP}^2 - v_o^2)^{-3/2} (1 - v_o^2) \qquad (3.22)$$

3) Calculate magnitude and phase of the integral:

$$\text{MAG} = S_x(f, \text{UOSP}) \sqrt{2\pi / \text{DRV2ND}} \qquad (3.23)$$

$$\text{PHASE} = -k_n [\Delta X_i \text{UOSP} + (1 - \text{UOSP}^2 - v_o^2)^{1/2} \Delta Z] + \frac{\pi}{4}$$

Note that the integral is a function of v_o and the indices i and n through k_n and ΔX_i. The dependence of the magnitude

34

on the index n is negligible, thus DRV2ND is calculated for all n using k_o. We will denote the integral by $IWRTUO(v_o, k_n, i)$.

The numerical method using the Euler summation can also be applied to the integration w.r.t. u_o. This numerical method is implemented to verify the result of the stationary phase method and extend application of the program to larger cross ranges. The applicability of the method can be shown by separating the integrand of equation (3.4) into a real and imaginary part

$$\int_{-1}^{1} (S_x(f, u_o) \cos\{-k_n[u_o \Delta X_i + (1 - u_o^2 - v_o^2)^{1/2} \Delta Z]\}$$

$$\tag{3.25}$$

$$+ jS_x(f, u_o) \sin\{-k_n[u_o \Delta X_i + (1 - u_o^2 - v_o^2)^{1/2} \Delta Z]\}) du_o$$

As shown above, the point of main contribution to the integral in equation (3.25) is the stationary point UOSP. Away from this point the integrand becomes more and more oscillatory and consequently more difficult to integrate numerically. One would therefore like to use a scheme in which the size of the subintervals is dependent on the behavior of the integrand. The method described in III.B.1.c uses the zero crossings of the integrand as points of separation, thus making sure that the integrand within a subinterval is "well-behaved" and can be efficiently integrated by standard numerical methods. This division into "well-behaved" subintervals could also be obtained by using the relative extremes as points of separation. The integrand of equation (3.25)

35

has closed form solutions to the zero crossings and relative

extremes of both the real and imaginary parts. The zero

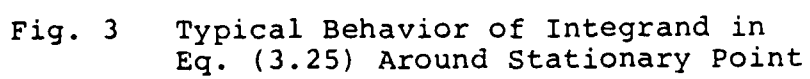crossings of the imaginary part of the integrand are found

by solving:

$$-k_n \Delta X_i u_o - k_n \Delta Z (1 - u_o^2 - v_o^2)^{1/2} = n\pi \; ; \quad \text{n integer} \quad (3.26)$$

or

$$u_o = \frac{-\Delta X_i (n\pi) \pm \Delta Z [(1 - v_o^2) k_n^2 (\Delta X_i^2 + \Delta Z^2) - (n\pi)^2]^{1/2}}{k_n (\Delta X_i^2 + \Delta Z^2)} \quad (3.27)$$

These also are the locations of the relative extremes

of the cosine term appearing in the real part of the integrand.

In order to avoid integrating the real and imaginary parts

of the integral separately, the same subintervals are used

for both the real and imaginary parts of the integral. Points

of separation for the subintervals are the zero crossings of

the imaginary part of the integrand, which coincide with the

relative extremes for the real part of the integrand. As a

starting point for the integration, define the first subinter-

val using the point of main contribution, i.e., the stationary

point UOSP.

Fig. 3 shows a typical behavior of the real and imagin-

ary parts of the integrand around the stationary point. The

figure also indicates the position of the subintervals.

Integration of the successive subintervals (from UOSP outward),

will form alternating terms of decreasing magnitude for both

36

Fig. 3 Typical Behavior of Integrand in
Eq. (3.25) Around Stationary Point

37

the real and imaginary parts of the integral, making it possible to effectively speed up the convergence by using a complex Euler summation. The decreasing magnitude is caused by the non-linear behavior of the phase term and the decreasing amplitude of the integrand which is given by the transmit far-field directivity function $S_x(f,u_0)$. The program implements the following procedure:

1) Calculate the value of the stationary point UOSP according to equation (3.17). This value of u_0 also denotes the maximum (negative) value of the phase term.

2) Calculate NZ the maximum integer multiples of π contained in the maximum (negative) value of the phase term (see Fig. 3).

$$NZ = INTEGER\left(\left|\frac{-k_n[UOSP\Delta X_i + (1-UOSP^2-v_0^2)^{1/2}\Delta Z]}{\pi}\right|\right) \quad (3.28)$$

Note that NZ denotes the zero crossings of the imaginary part of the integrand nearest to the stationary point UOSP.

3) Calculate the values of u_0 for the zero crossings of the imaginary part of the integrand denoted by NZ using equation (3.27).

$$UOZ_{1,2} = \frac{-\Delta X_i(NZ\pi) \pm \Delta Z[(1-v_0^2)k_n^2(\Delta X_i^2+\Delta Z^2)-(NZ\pi)^2]^{1/2}}{k_n(\Delta X_i^2 + \Delta Z^2)}$$

$$(3.29)$$

Integrate the subinterval between these two values of UOZ.

4) Decrement NZ and calculate the values of $UOZ_{1,2}$, denoting the next zero crossings of the imaginary part of the integrand, by using the formula given in 3) above.

38

5) Define two subintervals, one on each side of the
    stationary point, from zero crossing to zero crossing
    for the imaginary part and from extreme to extreme
    for the real part of the integrand.

6) Integrate both subintervals and add the contribution
    to the total value of the integral using a complex
    Euler summation.

7) Check for convergence by comparing the difference
    between the last two values of the Euler summation
    with a tolerance. If not convergent, go back to 4)
    and repeat the procedure.

One more note can be made concerning the numerically
calculated value of the integral w.r.t. u_o for different k_n.
Recalculation of the whole integral for different values of
n would be very time consuming. We therefore introduce a
correction term to obtain values of the integral for $n \neq 0$,
based on the value of integral for n = 0. This correction
term is only of importance to the phase of the integral, the
effect of different values for k_n on the magnitude is
neglected. For n = 0 the stationary phase method results in
the following expression for the phase:

$$\text{PHASE } (n = 0) \quad = \quad -k_o [\Delta X_i \text{UOSP} + (1 - \text{UOSP}^2 - v_o^2)^{1/2} \Delta z] + \frac{\pi}{4} \quad (3.30)$$

Brekhovskikh [Ref. 14] demonstrates that taking into
account higher-order terms in the method of stationary phase
does change the amplitude but not the phase of the resulting
approximation. This shows that the point of main contribu-
tion, i.e., the stationary point determines the phase of the
integral. If the method of stationary phase is no longer

39

IV. COMPUTER SIMULATED DATA

This section describes the validation of the model. It presents and interprets the data generated by the computer model for a number of test cases.

A. PRESENTATION OF COMPUTER SIMULATED DATA

Data generated by the computer model consists of the frequency response matrix $H(f,i,q)$ and the output electrical signal at each element $y(t,i,q)$. Interpretation of the data is done directly by examining the frequency response $H(f,i,q)$ and by the use of a three-dimensional DFT program to calculate the Fourier transforms of the computer simulated output electrical signals w.r.t. time and space. The program is based upon 3-dimensional DFT beamforming for planar arrays as described by Ziomek [Ref. 4]. First a brief overview of the output from the 3-D DFT program is given.

The program calculates the 3-dimensional DFT of the electrical output signal from all receiver elements and is given by

$$Y_S(q,r,s) = \sum_{m=-M'}^{M'} \sum_{n=-N'}^{N'} \sum_{\ell=-L'}^{L'} c_m d_n y(\ell,m,n) \exp[-j2\pi q\ell/L] \cdot$$

$$\exp[j2\pi rm/(M+Mz)]\exp[j2\pi sn/(N+NZ)] \tag{4.1}$$

```
      DO 100 J = 1, N
100         COEF(NEW,J+1) = COEF(NEW,J) + COEF(OLD,J)
      FACTOR = FACTOR / 2
      EULSUM = EULSUM + COEF(NEW,N)/FACTOR
C     Prepare for next contribution
      SWAP( NEW, OLD )
```

The program implements this algoritm in complex form to perform N' summations simultaneously.

More details on the actual programming of the discussed numerical methods and flowcharts, data structures used, etc., is considered applied programming and will not be discussed in this thesis.

is described in III.A.2 for the integration w.r.t. v_o and is similar to the procedure used for the numerical integration w.r.t. u_o in Section III.A.2.

Implementation of the integration over a subinterval using the Newton Cote's formulas is straightforward and will not be examined in detail. The framework for this part of the program can be found in Squire [Ref. 13: p. 281].

The Euler summation is used to speed up convergence of the numerical integration. The objective is to form the sum

$$\frac{a_1}{2} + \frac{b_1}{4} + \frac{c_1}{8} + \frac{d_1}{16} \cdots .$$

from the original sequence $a_1, a_2, a_3, a_4, \ldots, a_n$ which are the contributions from the subintervals 1 through n, where

$$b_k = a_k + a_{k+1}, \quad c_k = b_k + b_{k+1}, \cdots .$$

The algorithm used is described below and uses an array COEF to store the coefficients a_n, b_{n-1}, c_{n-2}, d_{n-3}, $\cdots$ etc. The size of this array determines how many contributions can be handled.

```
      DIMENSION COEF(2,SIZE)

      REAL EULSUM,FACTOR

      INTEGER NEW, OLD

C     Add contribution N

      COEF (NEW,1) = N_th_CONTRIBUTION
```
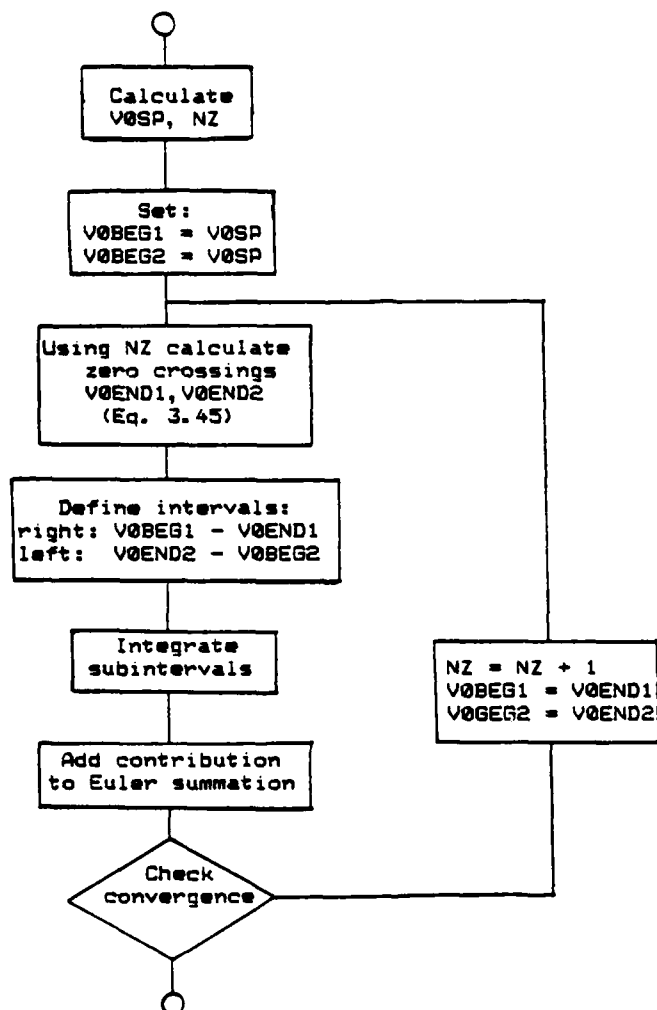
51

Fig. 6   Calculation of Subintervals by CALCHF
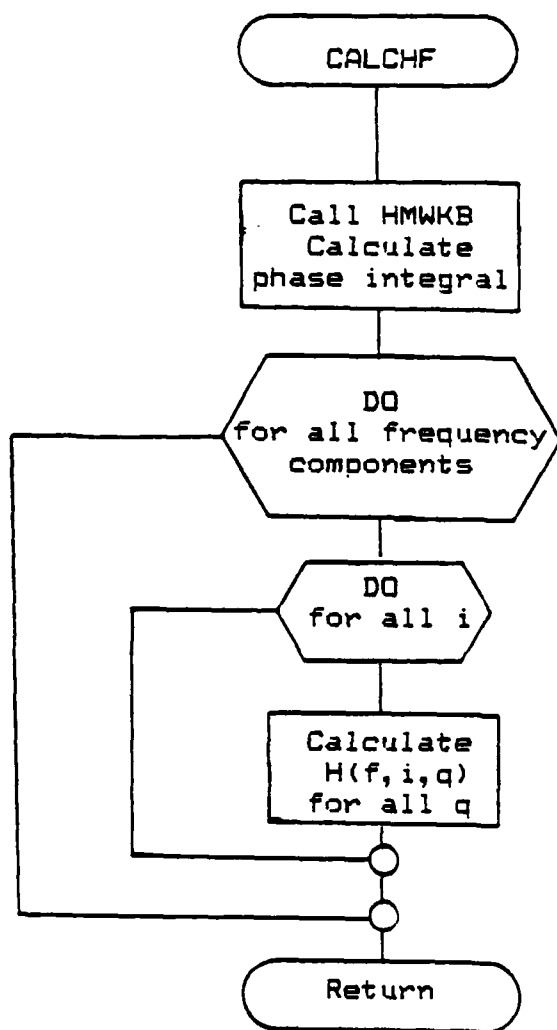
50

Fig. 5   Flowchart of Module CALCHF

49

integrations and keep track of N' Euler summations simultaneously. It does, however, also reduce some overhead. Convergence checking on the integration w.r.t. v_o is done only on the two outermost elements with indices $q = (N'-1)/2$ and $q = -(N'-1)/2$.

The calculation of those terms that multiply IWRTUO(k_n, v_o, i) in the summation given by equation (3.46) is simplified by precomputing part of the phase components of the ocean medium transfer function given by equations (3.36) and (3.37). The program does this in the subroutine HMWKB and stores the resulting phase integral values in an array. To obtain a particular value for the phase, the program only needs to multiply with the factor k_n/v_o. Especially in the case of a more complicated sound speed profile, the computation of the phase integrals can be involved and precomputation improves efficiency. The stated time-invariance of the model also forces precomputation since the random numbers used to model the phase term θ_{MR} can be drawn only once. The random numbers were obtained from the IMSL routine GNNML which was used to generate a series of $N \times N'$ random numbers with distribution $N(0,1)$. From these random numbers the different random phase terms θ_{MR} for all combinations (n,q) are readily computed using equation (3.37). Figure 5 shows a simple flowchart of the CALCHF module.

The innermost block which actually calculates H(f,i,q) is shown in more detail in Fig. 6. The diagram shows how the subintervals are defined by the program. The procedure followed

48

Most important numerical calculations required by the model are done within the module CALCHF. The module CALCHF calculates the frequency response matrix $H(f,i,q)$, i.e., the frequency response for all receiver elements (i,q). This mainly involves evaluation of the double integral w.r.t. u_o and v_o. It has two versions dependent on the integration technique used to evaluate the integral w.r.t. u_o:

CALCHF_1   Use stationary phase method to integrate w.r.t. u_o.

CALCHF_2   Use numerical technique to integrate w.r.t. u_o.

To avoid recalculation and improve program efficiency the outer integration w.r.t. v_o is done simultaneously for all elements with the same index i. This is particularly important when using the more time consuming numerical method to integrate w.r.t. u_o. This can be done by separating the summation inside the integrand into a part dependent on q and a part dependent on i. Recall that equation (3.35) gives the form of the integrand as follows:

$$\sum_{n=-(N-1)/2}^{(N-1)/2} d_n H_M(k_n, v_o, n, q) \exp\{-jk_n v_o \Delta Y_{qn}\} IWRTUO(v_o, k_n, i) \qquad (3.46)$$

So given a value for IWRTUO for a given index i we can evaluate the integrand for all values of q, thus avoiding recalculating the most computation intensive part. This scheme does result in more complex coding. The program has to do N'
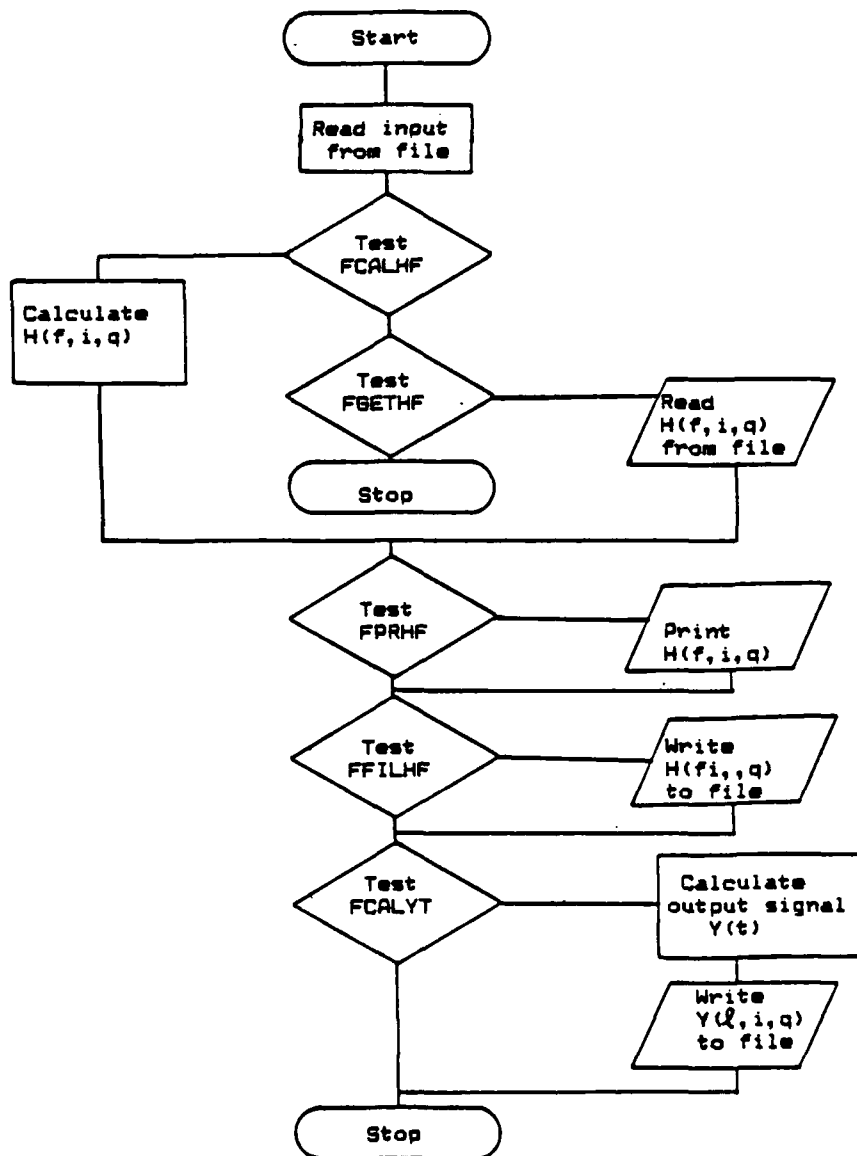
Fig. 4   Flowchart of Main Program Module

46

B. PROGRAM OUTLINE

The flowchart in Fig. 4 gives an overview of the program logic. This logic is controlled by flags which are read from the input data file together with all program parameters. The program parameters determine:

- Model geometry: x_o, y_o, z_o, x_r, y_r, z_r, M, N, M', N', d_x, d_y, d_x', d_y'.

- Speed of sound profiles: c_o, g, σ.

- Beam steering angles for the transmit array and the frequency to be used for the beam steering calculations.

- The fundamental period T_o of the electrical input signal and the total number of samples L in the electrical output signal. The program determines the sampling period $T_s = T_o/L$ and calculates the output electrical signal at time instants

$$-(L-1)T_o/2, \ldots, 0, \ldots, (L-1)T_o/2$$

- The values of the frequency components in the electrical input signal and their complex Fourier series coefficients c_k.

- Tolerance values ERRORU and ERRORV for the numerical integrations w.r.t. u_o and v_o. The user should validate his choice for the tolerance values by comparing them against the absolute values calculated by the program for the integrations.

Processing is done in accordance with flag settings and allows for a number of options:

- The frequency response H(f,i,q) can be calculated or read from a previously created file.

- The calculated frequency response H(f,i,q) can be filed for later use and/or printed.

- The output electrical signal can be calculated and filed for further processing by other programs.

45

described for the integration w.r.t. u_o. The point of main contribution is approximately where the phase term $\alpha(v_o)$ is stationary. This point is used to begin the numerical integration. The stationary point VOSP is given by

$$VOSP = \Delta Y / (R_{ri}^2 + \Delta Y^2)^{1/2} \qquad (3.43)$$

which is a solution of $\alpha'(VOSP) = 0$ where R_{ri} is the radial distance from the center of the transmit array to a receiver element with index i and is given by

$$R_{ri} = (\Delta X_i^2 + \Delta Z^2)^{1/2} \qquad (3.44)$$

The points of separation for the integral can be found by

$$VOZ_{1,2} = \frac{-\Delta Y(n\pi) \pm R_{ri}[k_o^2(\Delta Y^2 + R_{ri}^2) - (n\pi)^2]^{1/2}}{k_o(R_{ri}^2 + \Delta Y^2)} \qquad (3.45)$$

Another method using a brute force technique was used to validate the above described procedure. This method integrates w.r.t. direction cosine v_o between user specified limits of integration. It divides the range of integration into subintervals of equal size which are integrated by a standard routine as described above in III.A.1.b. Both methods agreed numerically although the method using the unequally spaced subintervals and the Euler summation was much more efficient in terms of computation time.

where $\Delta Y = y_r - y_o$. If we let

$$X(v_o) = \sum_{n=-(N-1)/2}^{(N-1)/2} d_n H_M(k_n, v_o, n, q) \exp\{-jk_n v_o (qd_y' - nd_y) + \frac{\pi}{4} + \Delta\phi\} \cdot$$

$$\exp\{-j(k_n - k_o)[\Delta Y v_o + \Delta X_i UOSP + (1 - UOSP^2 - v_o^2)^{1/2} \Delta Z]\} \cdot |IWRTUO(v_o, k_n, i)| \quad (3.40)$$

and

$$\alpha(v_o) = -k_o[\Delta Y v_o + UOSP\Delta X_i + (1 - UOSP^2 - v_o^2)^{1/2} \Delta Z]$$

$$(3.41)$$

$$\alpha(v_o) = -k_o[\Delta Y v_o + (1 - v_o^2)^{1/2} \sqrt{\Delta X_i^2 + \Delta Z^2}]$$

Then the integral given by equation (3.39) becomes:

$$\int_{a_q}^{1} X(v_o) \exp[j\alpha(v_o)] \, dv_o$$

where $X(v_o)$ is slowly varying compared to $\exp\{j\alpha(v_o)\}$. The

phase term $\alpha(v_o)$ can now be used to define subintegrals which

are "well behaved." This is accomplished by taking the roots

of $\sin(\alpha(v_o))$ or $\cos(\alpha(v_o))$ as the points of separation between

the different subintervals. Contributions from the subintegrals

are in general of decreasing magnitude and alternating sign,

so the Euler summation can be used to effectively speed up

convergence.

The implemented procedure uses the roots of $\sin(\alpha(v_o))$

as the points of separation and is similar to the one already

v_o. The expressions within the square brackets for θ_{MD} and θ_{MR} are only dependent on the geometry and can be precomputed. A random number generator was used to generate a series of $N(0,1)$ distributed numbers to be used for n_{NR} in equation (3.37).

Because of the complexity of the total phase term in the integrand of equation (3.35), a closed form approximation could not be found. The numerical method used is also based on the procedure given in III.A.1.c. The integral is divided into subintegrals in such a way that the subintegrals are all "well behaved." The problem is to find a general form which approaches the phase of the integrand. This form can then be used to calculate the points of separation in order to define the subintervals. We will proceed by separating the phase term of the integrand into a major part and a minor slowly varying part. Combining the phase term of the integral w.r.t. u_o given by equation (3.32) with equation (3.35) results in the following expression for the integration w.r.t. v_o:

$$\int_{a_q}^{1} \sum_{n=-(N-1)/2}^{(N-1)/2} d_n H_M(k_n, v_o, n, q) \exp\{-jk_n v_o (q d_y' - n d_y) + \frac{\pi}{4} + \Delta\phi\} \cdot$$

$$\exp\{-j(k_n - k_o)[\Delta Y v_o + \Delta X_i \text{UOSP} + (1-\text{UOSP}^2 - v_o^2)^{1/2} \Delta Z]\} \cdot$$

$$|\text{IWRTUO}(v_o, k_n, i)| \exp\{-jk_o [v_o \Delta Y + \text{UOSP} \Delta X_i + (1-\text{UOSP}^2 - v_o^2) \Delta Z]\} dv_o \qquad (3.39)$$

where we used $c_O = 1500$ m/sec and $g = 0.017$ 1/sec. An upper limit for the correction term is $(k_n - k_O) \Delta Z$ if $\Delta Z \gg \Delta X$.

Having established two methods to implement the calculation of the inner integral w.r.t. direction cosine u_O, the outer integral w.r.t. direction cosine v_O is now considered. The integral can be written as [see equation (3.6)]:

$$\int_{a_q}^{1} \sum_{n=-(N-1)/2}^{(N-1)/2} d_n H_M(k_n, v_O, n, q) \exp[-jk_n v_O \Delta Y_{qn}] \text{IWRTUO}(v_O, k_n, i) dv_O$$

(3.35)

The ocean medium transfer function values are calculated with the use of equations (2.11), (2.16) and (2.18). Note that the deterministic and random phase terms pertain to the case of a sound speed profile with a constant gradient. In applying these formulae, we have to take into account that the source depth for a transmit element is not y_O but $y_O + ndy$. This results in the following formulae which were actually implemented:

$$A_M = (k_O v_O)^{-1/2}$$

(3.36)

$$\theta_{MD}(n,q) = \frac{k_n}{2v_O} \left[\frac{c_n}{g} \left(\frac{c_n}{c(y_r + qd_y')} - 1 \right) + \Delta Y_{qn} \right]$$

(3.37)

$$\theta_{MR}(n,q) = \frac{k_n}{v_O} \left[\frac{c_n}{g} \sigma n_{NR} \ln \left(\frac{c_n}{c(y_r + qd_y')} \right) \right]$$

(3.38)

We note that both the amplitude and phase terms depend on the value of the wavenumber k_n and direction cosine

valid we can write a general form for the phase based on equation (3.30):

$$\text{PHASE } (n = 0) = -k_o[\Delta X_i \text{UOSP} + (1 - \text{UOSP}^2 - v_o^2)^{1/2} \Delta Z] + \frac{\pi}{4} + \Delta\phi \tag{3.31}$$

where $\Delta\phi$ represents some unknown correction term. This relies on the fact that the stationary point UOSP is always very close to the point of main contribution. Based on this, the phase term for $n \neq 0$ can be written as:

$$\text{PHASE}(n) = -[k_o + (k_n - k_o)][\Delta X_i \text{UOSP} + (1 - \text{UOSP}^2 - v_o^2)^{1/2} \Delta Z] + \frac{\pi}{4} + \Delta\phi \tag{3.32}$$

where

$$(k_n - k_o)[\Delta X_i \text{UOSP} + (1 - \text{UOSP}^2 - v_o^2)^{1/2} \Delta Z] \tag{3.33}$$

represents the correction term which is readily computed for different values of n. This phase correction term has to be added to the phase for $n = 0$ to obtain phase values for $n \neq 0$. Note that this correction term is only important for larger ranges ΔZ, assuming that $\Delta Z \gg \Delta X$. This can be seen by calculating a typical value for $k_n - k_o$, where the element spacing is taken as $\lambda/2$ and the sound speed profile has a constant gradient g:

$$k_n - k_o = 2\pi f\left(\frac{1}{c_n} - \frac{1}{c_o}\right) \approx -\frac{\pi g}{c_o} n = 3.6 \times 10^{-5} n \tag{3.34}$$

where:

L: total number of time samples in one fundamental period T_O of the signal.

$L' = (L-1)/2$

T_s: sampling period

M: total odd number of elements in the x-direction in the receive array

$M' = (M-1)/2$

N: total odd number of elements in the y-direction in the receive array

$N' = (N-1)/2$

d_x, d_y: spacing in x- and y-directions, respectively.

c_m, d_n: complex separable weights for the array given by

$$c_m = a_m \exp\{j\theta_m\}$$

$$d_n = b_n \exp\{j\phi_n\}$$

q,r,s: binnumbers of the DFT which are related to values of frequency f, direction cosine u and direction cosine v, respectively.

$y(\ell,m,n)$: output electrical signal at time instant ℓT_s at element (m,n) of the receive array.

MZ, NZ: Number of zeros used for padding to increase the resolution of the direction cosines u and v, respectively.

Note that the symbols used to characterize this planar receive array are not the same symbols used to describe the receive array in the computer model (II.A.1). Rectangular amplitude weighting without beam steering is used for all the results presented in this chapter.

In II.B.3 we made the constraint to represent the transmit electrical signal by a finite Fourier series with maximum frequency $KMAX \cdot f_o$. Thus, to avoid aliasing, we must sample the received signal with a sample rate equal to or greater than the Nyquist rate:

$$f_s \geq 2 \, KMAX \, f_o \; ; \quad T_o \geq 2 \, KMAX \, T_s \qquad (4.2)$$

The total number of samples L to be taken in order to avoid aliasing must obey the following inequality:

$$L \geq 2 \, KMAX + 1 \qquad (4.3)$$

The sampling period is determined by:

$$T_s = T_o/L \qquad (4.4)$$

The program evaluates the 3-dimensional summation in three steps. The first step is to perform a DFT w.r.t. time at each receiver element (m,n). If the sound field incident upon the array is a general plane wave, then the received electrical signal can be expressed by

$$y(\ell,m,n) = g(\ell T_s - t_o)$$

where $t_o = (u_o m d_x + v_o n d_y)/c$ denotes the time delay between the signals at the different elements. The DFT w.r.t. time becomes

55

$$Y_S(q,m,n) = c_m d_n \sum_{\ell=-L'}^{L'} g(\ell T_S - t_o) W_L^{q\ell} \qquad (4.5)$$

where $W_L^{q\ell}$ is the factor $\exp\{-j2\pi q\ell/L\}$. Using the above stated fact that the received signal is given by a finite Fourier series, we obtain

$$Y_S(q,m,n) = c_m d_n L c_q \exp\{-j2\pi q f_o (u_o m d_x + v_o n d_y)/c\} \qquad (4.6)$$

A normalized expression is defined by

$$Y_{SN}(q,m,n) = Y_S(q,m,n,)/(c_m d_n L)$$

$$= c_q \exp\{-j2\pi q f_o (u_o m d_x + v_o n d_y)/c\} \qquad (4.7)$$

So $Y_{SN}(q,m,n)$ allows us to estimate the amplitude of the frequency components in the signal at each element (m,n).

The next DFT calculation is:

$$Y_S(q,r,n) = \sum_{m=-M'}^{m'} Y_S(q,m,n) \exp\{j2\pi mr/(m+mZ)\} \qquad (4.8)$$

where we have padded with NZ zeros to increase resolution. Substitution equation (4.6) into equation (4.8) leads to

$$Y_S(q,r,n) = L c_q d_n \exp\{-j2\pi q f_o v_o n d_y/c\} \cdot$$

$$\sum_{m=-M'}^{M'} c_m \exp\{-j2\pi q f_o u_o m d_x/c\} W_{M+MZ}^{rm} \qquad (4.9)$$

56

and a normalized expression can be written as

$$Y_{SN}(q,r,n) = c_q \exp\{-j\, 2\pi q\, f_o\, v_o\, n\, d_y/c\} \cdot$$

$$\sum_{m=-M'}^{M'} c_m \exp\{-j 2\pi\, q\, f_o\, u_o\, m\, d_x/c\} W_{M+MZ}^{rm} / \sum_{m=-M'}^{M'} a_m \qquad (4.10)$$

This expression is directly proportional to the Fourier series coefficients c_q and to the normalized far-field beam pattern at a frequency $q \cdot f_o$ of a line array consisting of M elements which is lying along the X-axis. The planar array has N such line arrays as indicated by the index n. If no beam steering is done ($c_m = a_m$), then $Y_{SN}(q,r,n)$ has a maximum approaching c_q at the bin number related to the direction cosine value which is closest to u_o. The DFT bin number r is related to the direction cosine value by

$$u = r\lambda/[(M+MZ)d_x] ; \qquad \lambda = c/qf_o \qquad (4.11)$$

This value of u is an estimate of u_o. Therefore, for each frequency component of a plane wave propagating in the u_o, v_o direction, the expression given by equation (4.10) can be used to estimate the magnitude of the frequency component and the direction cosine u_o. An estimate of v_o can be obtained in the same way by evaluating

$$Y_{SN}(q,m,s) = c_q \exp\{-j2\pi q f_o u_o m d_x/c\} \cdot$$

$$\sum_{n=-N'}^{N'} d_n \exp\{-j2\pi q f_o v_o n d_y/c\} W_{N+NZ}^{sn} / \sum_{n=-N'}^{N'} b_n \quad (4.12)$$

The above mentioned estimates of c_q, u_o and v_o are provided by the program in the form of printouts of $Y_{SN}(q,m,n)$, $Y_{SN}(q,r,n)$ and $Y_{SN}(q,m,s)$. The printouts are done for user specified values of m and n. No padding with zeros is done for the transform w.r.t. time. Padding for the spatial transforms is done to obtain a user specified step size in direction cosine u or v. Graphical output for estimation of u_o and v_o was also obtained. The complete three-dimensional transform $Y_S(q,r,s)$ was used to produce a three-dimensional plot to aid in interpretation and for illustrative purposes. The estimates of u_o and v_o can also be used to calculate estimates of the spherical angles denoting the direction of the sound source as measured from the center of the receive array. These angles are also referred to as target bearing and elevation angles. The estimates are given by

$$\hat{\psi}_o = \tan^{-1}(\hat{v}_o/\hat{u}_o) \quad (4.13)$$

$$\hat{\theta}_o = \sin^{-1}([\hat{u}_o^2 + \hat{v}_o^2]^{1/2}) \quad (4.14)$$

where $\hat{\psi}_o$ and $\hat{\theta}_o$ are estimates of the target bearing and elevation angles, respectively. Note that an error in the

58

estimation of either u_O or v_O or both affects both the target bearing angle and target elevation angle estimates.

B. TEST CASES

Most test cases run by the model are kept simple to aid in interpretation. All cases are run first in a deterministic homogeneous medium so that results could be easily interpreted and compared to known methods and approximations. All test cases are checked to obey the criteria required by the transfer function.

The values of the basic parameters such as source depth y_O, gradient g and reference speed of sound c_O were chosen in order to model the wave propagation between a source located on the SOFAR channel axis and a deep receiver. At moderate latitudes from 60°S to 60°N the speed of sound on the SOFAR axis ranges from 1450-1485 m/sec in the Pacific and from 1450-1500 m/sec in the Atlantic [Ref. 15]. The depth of the SOFAR axis is typically between 1000 and 1200 m at moderate latitudes [Ref. 15]. The gradient below the SOFAR axis is given by g = 0.017 1/sec [Ref. 19]. Values for the standard deviation σ of the random component of the index of refraction range from 0.25×10^{-4} [Refs. 17,18] to 1.0×10^{-4} [Ref. 16]. These values were used in choosing representative parameters for the following test cases:

1. Homogeneous Cases

As a baseline test case we define the deterministic homogeneous case HMG1:

c_o = 1475 m/sec.

g = 0: constant speed of sound.

σ = 0: deterministic medium.

M = 11, N = 11: a 11 by 11 element transmit array with rectangular amplitude weighting in both the x and y directions.

M' = 5, N' = 5: a 5 by 5 element receive array.

x_o = 0.0   m x_r = 0.0   m

y_o = 1000.0 m y_r = 2000.0 m

z_o = 0.0   m z_r = 1732.05 m

$d_x = d_y = d'_x = d'_y$ = 0.7375 m: spacing equal to $\lambda_{min}/2$.

θ_r = 30°, ψ_r = 90°: spherical angles denoting the line of sight between the center of the transmit array and the center of the receive array.

u_r = 0, v_r = 0.5: line of sight direction cosine values from the center of the transmit array to the center of the receive array.

u_b = 0, v_b - 0.5: direction cosine values used to steer the main lobe of the transmit far-field beam pattern towards the center of the receive array.

KMAX = 1: single frequency component.

f_o = 1000 Hz, T_o = 0.001 sec.

$c_1 = a_1$ = 1.0: complex Fourier series coefficient equals 1.

L = 3: 3 times samples per fundamental period T_o.

Based on the definition of test case HMG1 we define the following cases:

HMG2: Same as HMG1 except

x_r = 200 m, z_r = 1720.464 m

$u_r = u_b$ = 0.1, $v_r = v_b$ = 0.5

θ_r = 30.66°, ψ_r = 78.69°.

HMG3: Same as HMG1 except

$$y_r = 1500 \text{ m}, \qquad z_r = 866.0246 \text{ m}$$

HMG4: Same as HMG1 except

$$y_r = 2500 \text{ m}, \qquad z_r = 2598.074 \text{ m}$$

HMG5: Same as HMG1 except

$$d_x = d_y = d_x' = d_y' = .36875 \text{ m}$$

$$f_o = 2000 \text{ Hz}, \qquad T_o = 0.0005 \text{ sec.}$$

HMG6: Same as HMG1 except

$$x_r = 1224.745 \text{ m} \qquad z_r = 1224.745 \text{ m}$$

$$u_r = u_b = 0.6124, \qquad v_r = v_b = 0.5$$

$$\theta_r = 52.24°, \qquad \psi_r = 39.23°.$$

HMG7: Same as HMG1 except

$$d_x = d_y = d_x' = d_y' = 0.184375 \text{ m}$$

$$f_o = 4000 \text{ Hz}, \qquad T_o = 0.00025 \text{ sec.}$$

HMG8: Same as HMG2 except

KMAX = 5: five frequency components.

$$f_o = 1000 \text{ Hz}, \qquad T_o = 0.001 \text{ sec.}$$

$$f_{max} = 5000 \text{ Hz.}$$

f_b = 3000 Hz: frequency used for steering the transmit beam pattern.

$$d_x = d_y = d_x' = d_y' = 1475/2 \; f_{max} = 0.1475 \text{ m}$$

$c_k = a_k = 1.0; \quad k = 1,2,\ldots,5:$ all complex Fourier series coefficients equal 1.

$L = 11:$ 11 time samples per fundamental period T_o.

2. Deterministic Inhomogeneous Cases

The following deterministic inhomogeneous cases incorporate a sound speed profile with a constant gradient. The definitions are based on those used for the homogeneous cases.

61

INHMG1, INHMG2, and INHMG5: Same as HMG1, HMG2 and HMG5 except

g = 0.017 1/sec.

INHMG8: Same as HMG8 except

g = 0.017 1/sec.

3. Random Inhomogeneous Cases

The following cases with an index of refraction composed of a deterministic and a random component are defined:

RINHMG1, RINHMG2: Same as INHMG1, INHMG2 except

$$\sigma = 1.0 \times 10^{-4}$$

RINHMG8: Same as INHMG8 except

$$\sigma = 0.25 \times 10^{-4}$$

C. RESULTS

This section will present and discuss the results from the computer model runs on the test cases as defined in Section IV.B. Some cases were run using both methods of integration w.r.t. u_o. The two methods showed no significant differences.

First, some trivial checks were made using the various homogeneous cases. Note, that all test cases have the same line of sight direction cosine v_r. For the homogeneous cases with a single frequency component of 1000 Hz the amplitude and phase terms of the ocean transfer function are equal and given by:

$$A_M = (k_o v_o)^{-1/2} , \qquad \theta_{MD} = 0 \qquad (4.15)$$

62

Since those cases have the same ocean transfer function values, the difference in the magnitude of the frequency response $H(f,i,q)$ for the various cases should only depend on the total range given by

$$R_{total} = \sqrt{(x_r - x_o)^2 + (y_r - y_o)^2 + (z_r - z_o)^2} \quad (4.16)$$

and the transmit far-field beam pattern. Cases HMG1, HMG3 and HMG4 also have the same line of sight direction cosine value u_r, so the influence of the transmit far-field beam pattern is the same for these cases and magnitude differences between the frequency responses can only depend on the total range and should behave in accordance with the expected spherical spreading for a homogeneous medium. Table IV.1 shows cases HMG1, HMG3 and HMG4 together with their total range and the magnitude of the frequency response at the center element of the receive array, i.e., $|H(f,0,0)|$. We conclude that the magnitude indeed falls off as $1/r$, only the total range is of importance.

Table IV.2 shows cases HMG1, HMG2 and HMG6 which differ only in cross range $x_r - x_o$ and line of sight direction cosine value u_r but have the same total range. In these cases only the far-field beam pattern can cause differences in the magnitude of the frequency response. The table shows that as the cross range increases the magnitude falls off, which is consistent with the fact that when a beam pattern is steered towards end-fire (to larger values of u_b and v_b) the

63

directivity index decreases due to the increasing beamwidth of the main lobe.

Table IV.3 shows the difference in magnitude of the frequency response at the center of the receive array between HMG1, HMG5, and HMG7. Cases with the same geometry but a different value for the single frequency component. This difference in magnitude is due to the frequency dependent amplitude factor inherent in the WKB approximation, which is not exact for a homogeneous medium.

Table IV.4 compares the magnitudes of the frequency response between the homogeneous cases HMG1, HMG2, and HMG5 and their inhomogeneous counterparts INHMG1, INHMG2 and INHMG5. We see that the magnitudes for the inhomogeneous cases are slightly lower, an expected phenomena because of the channeling effect in the inhomogeneous medium. In a medium with a constant positive gradient, the acoustic rays are bent upwards and the sound intensity decreases with increasing depth. This causes a lower magnitude of the acoustic signal then expected by spherical spreading only.

We will now present numerical and graphical output from the three dimensional DFT beamforming program. The frequency transform for the single frequency component cases simply reveals the magnitude of the transfer function multiplied by the amplitude of the input electrical signal and is not shown here. Figures 7 through 10 show the magnitude of the spatial DFT w.r.t. x, i.e., $Y_{SN}(q,r,n)$ versus direction cosine u, and

the magnitude of the spatial DFT w.r.t. y, i.e., $Y_{SN}(q,m,s)$

versus direction cosine u, for the cases HMG1, HMG2, INHMG1

and INHMG2. These graphs allow us to estimate the direction

of propagation of the incoming plane wave by finding the

coordinates of the maxima on the graphs. Tables IV.5 to

IV.8 provide numerical values for the above mentioned DFT's

w.r.t. x and y. They show values of $Y_{SN}(q,r,n)$ and $Y_{SN}(q,m,s)$

around the maxima and make it possible to form more accurate

estimates.

From the estimated values $\hat{u}_o$ and $\hat{v}_o$, we can calculate

estimates of target elevation angle $\hat{\theta}_o$ and target bearing

angle $\hat{\psi}_o$. Table IV.9 gives the results for the different

cases. The values of the estimators $\hat{u}_o$ and $\hat{v}_o$ were determined

by performing a second order interpolation on the data given

in tables IV.5 through IV.8. It is seen that the estimates

of target angles for the homogeneous cases are correct and

equal the line of sight angles from the receiver to the trans-

mitter. The estimated target angles for the deterministic

inhomogeneous cases deviate slightly from the line of sight

angles. This is due to the positive sound speed gradient

which causes upward bending of the acoustic rays so the direc-

tion cosine v_o, directly related to the vertical angle of

propagation of the plane wave, decreases as the wave travels

along. The net effect for these cases is relatively small

but noticable.

The effect of randomness, characterized by a random component

in the index of refraction with a standard deviation of

$\sigma = 1.0 \times 10^{-4}$ is examined next. Figure 11 shows estimates of u_O and v_O for the case RINHMG1 and Fig. 12 shows estimates of v_O for cases RINHMG1 and RINHMG2. As can be seen, the estimate of u_O is not influenced, which follows readily from the fact that the randomness is only present in the y direction. The estimate of v_O as shown in Fig. 12 for the case RINHMG2 shows the same random fluctuations as the one shown for case RINHMG1 in Fig. 11, since both cases used the same seed for the random number generator, resulting in the same random number sequence. Figure 12 also shows RINHMG1 with a different seed for the random number sequence. Although both are only two possible samples they clearly show the strong effect of the randomness on the beamformer output and the deterioration of the quality of the estimates (see Table IV.9).

Two three-dimensional plots are shown in Fig. 13, one for the deterministic inhomogeneous case INHMG2 and one for the random inhomogeneous case RINHMG2. These graphs illustrate the kind of output that can be obtained from the DFT beamformer, although it is difficult to accurately read off numerical values.

Finally, the cases HMG8, INHMG8 and RINGHM8, which involve several frequency components, are considered. The output for these cases is given in numerical and graphical form. Table IV.10 compares the Fourier series coefficients of the output electrical signal with the Fourier series coefficients of the transmitted electrical signal. The widely varying values are caused by:

1) The beam pattern of the transmit array is frequency
dependent. The differences between the transmitted frequency
components are relatively large and cause large differences in
amplitude c the Fourier series coefficients. The maximum
values are observed at f = 3000 Hz, i.e., the frequency for
which beam steering was done.

2) The deterministic inhomogeneous medium: As already
shown in other test cases the amplitude of the received signal
is frequency dependent due to the WKB approximation to the
wave equation in an inhomogeneous medium. Equation (2.10)
clearly shows the frequency dependence of the medium transfer
function.

3) The random inhomogeneous behavior of the medium: The
randomness introduces additional deviations. It can be seen
from table IV.10 that the effect of the randomness increases
with increasing frequency. Also, in the case of a random
medium, the estimation of the Fourier series coefficients
becomes strongly dependent on the location of the element in
the receive array. Note that table IV.10 only shows values
for the receive element (m = 0, n = 0).

The received angular spectrum for the different frequency
components of the cases INHMG8 and RINHMG8 is shown in Figs.
14 through 19. For the deterministic inhomogeneous case,
Figs. 14 through 16 show a regular behavior of the angular
spectrum according to the rectangular amplitude weighting
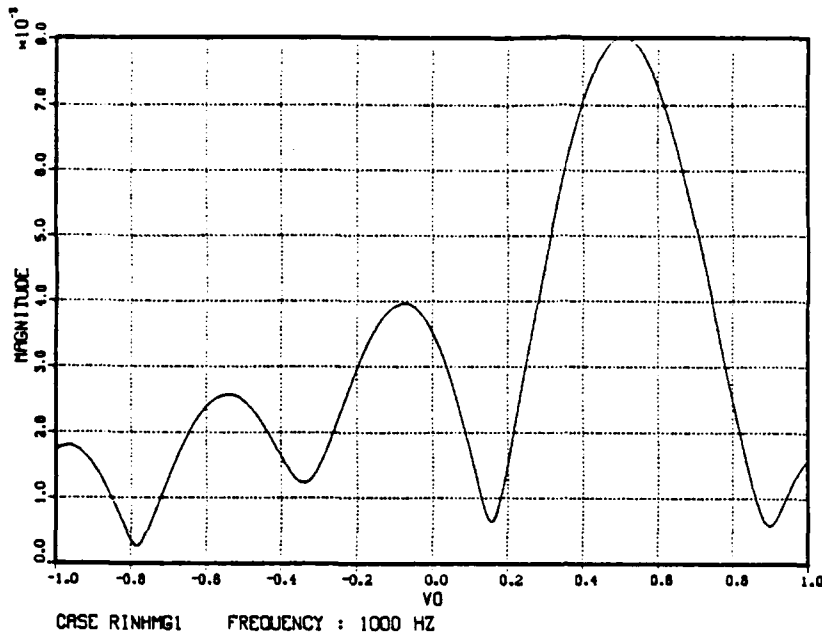used for the receive array. Estimation of u_o is exact.
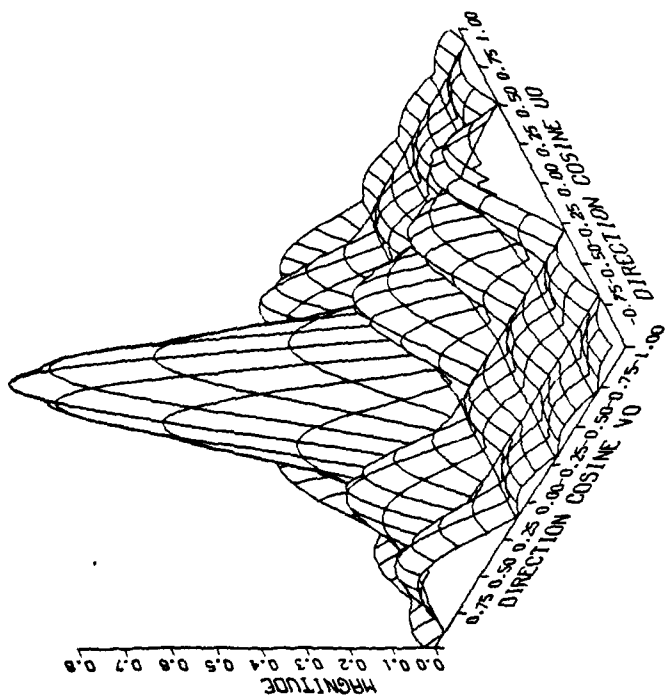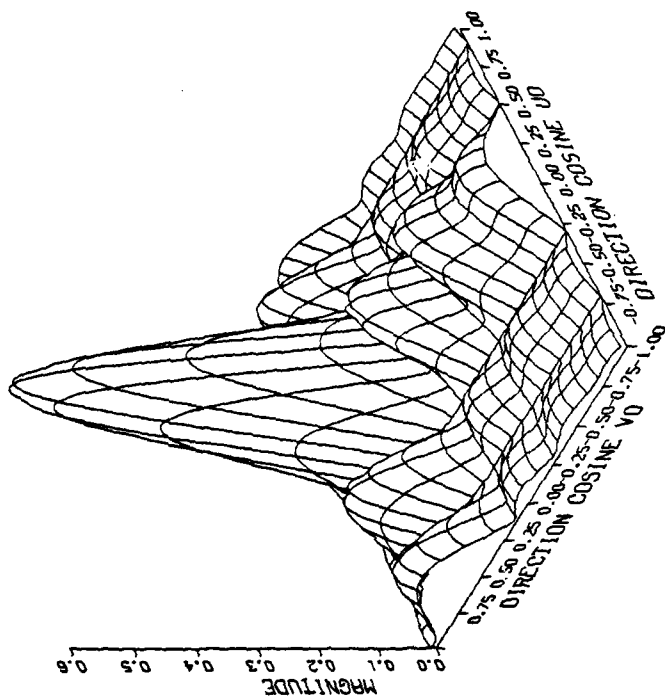
CASE INHMG2   FREQUENCY : 1000 HZ   CASE RINHMG2   FREQUENCY : 1000 HZ

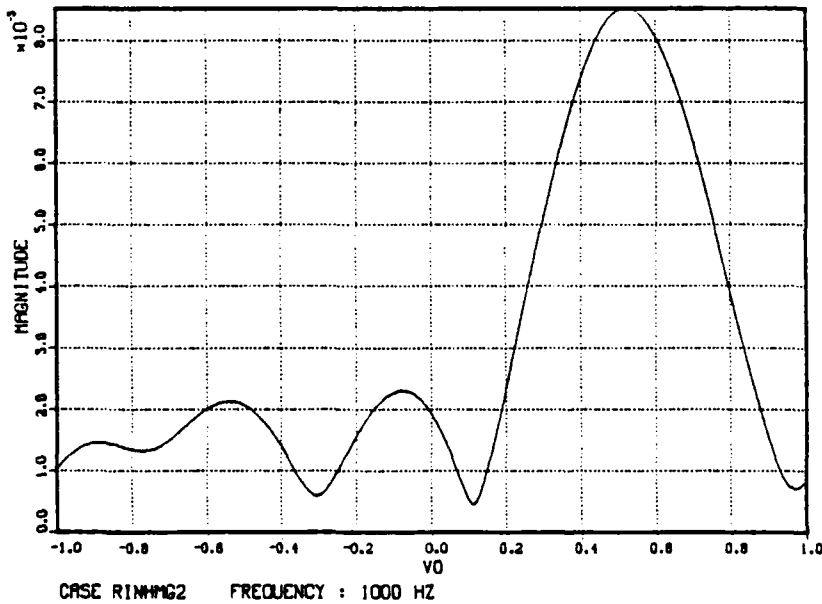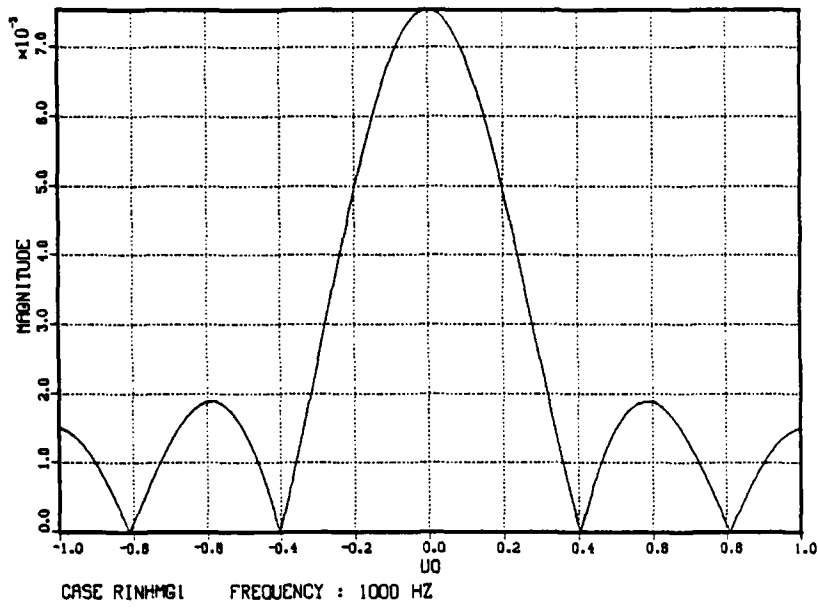Fig. 13 Angular Spectrum for Cases INHMG2 and RINHMG2

ESTIMATION OF VO

CASE RINHMG1   FREQUENCY : 1000 HZ

ESTIMATION OF VO

CASE RINHMG2   FREQUENCY : 1000 HZ

Fig. 12   Estimation of v for Cases RINHMG2 and
          RINHMG1 (Different Seeds)

ESTIMATION OF UO

CASE RINHMG1   FREQUENCY : 1000 HZ

ESTIMATION OF VO

CASE RINHMG1   FREQUENCY : 1000 HZ
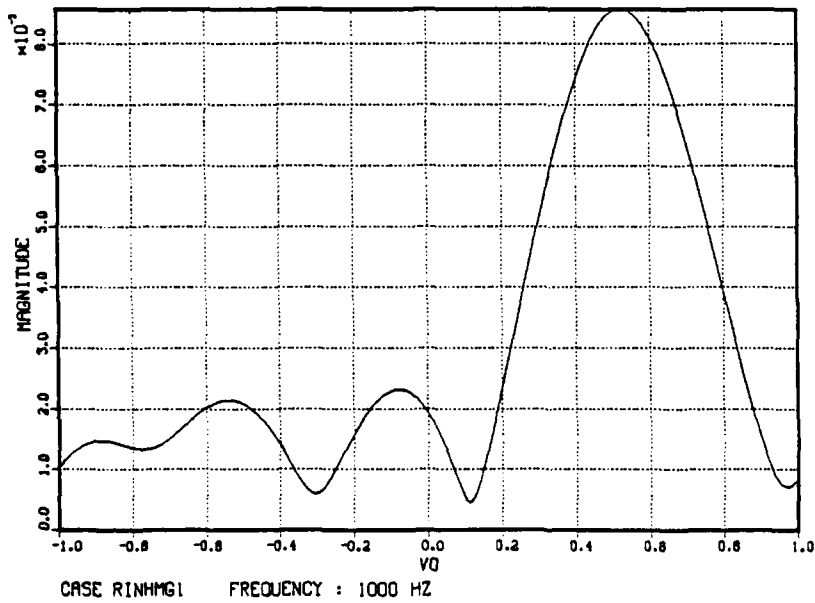
Fig. 11   Estimation of Direction of Propagation for
          Case RINHMG1

79

ESTIMATION OF U0

CASE INHMG2   FREQUENCY : 1000 HZ

ESTIMATION OF V0

CASE INHMG2   FREQUENCY : 1000 HZ
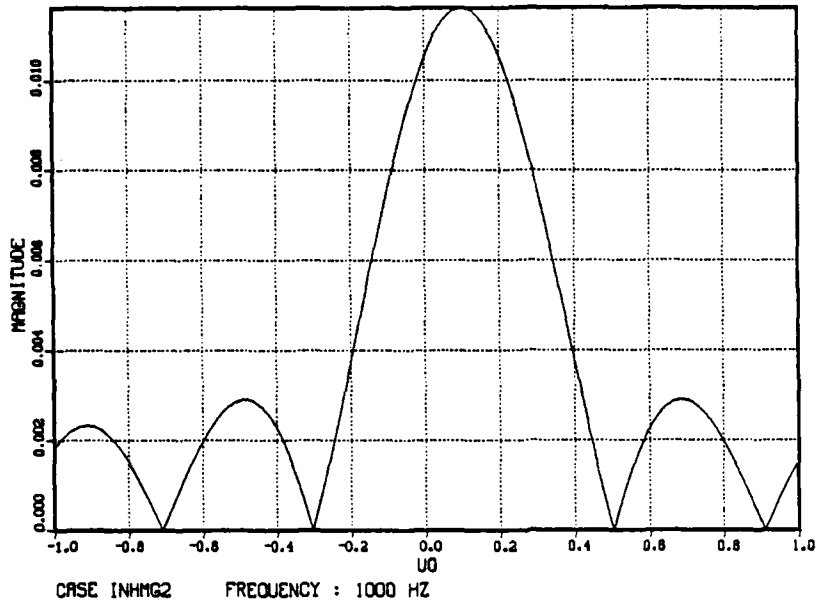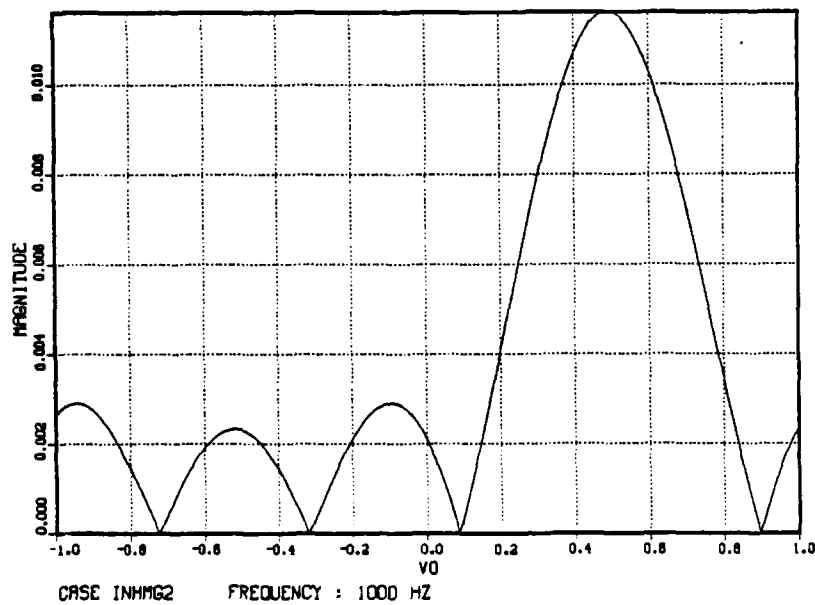
Fig. 10   Estimation of Direction of
Propagation for Case INHMG2
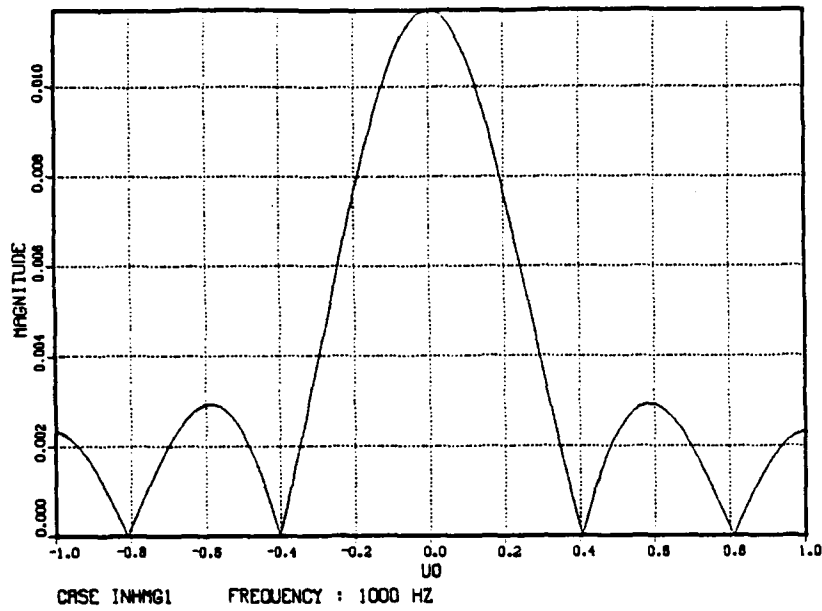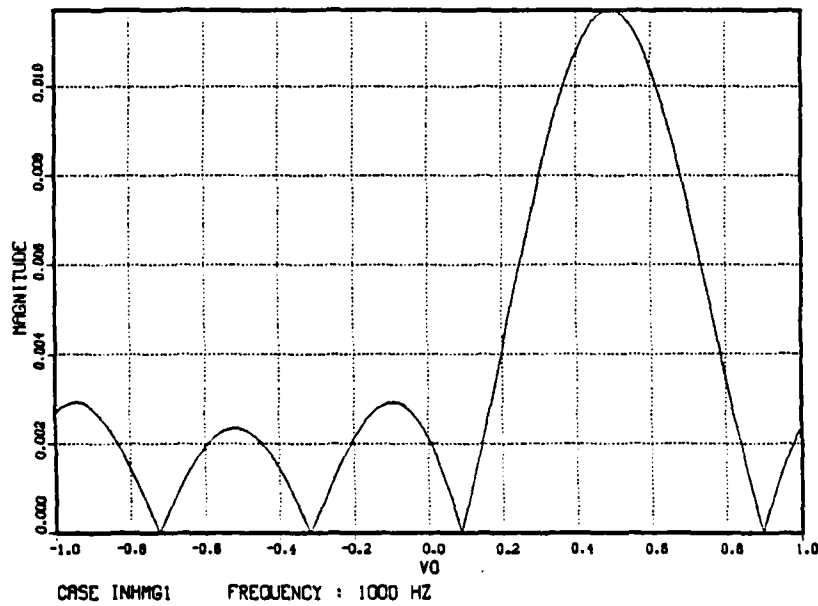
78

ESTIMATION OF UO

CASE INHMG1   FREQUENCY : 1000 HZ

ESTIMATION OF VO

CASE INHMG1   FREQUENCY : 1000 HZ

Fig. 9   Estimation of Direction of
          Propagation for Case INHMG1

77

ESTIMATION OF UO

CASE HMG2   FREQUENCY : 1000 HZ

ESTIMATION OF VO

CASE HMG2   FREQUENCY : 1000 HZ

Fig. 8   Estimation of Direction of
           Propagation for Case HMG2

76

ESTIMATION OF UO

CASE HMG1   FREQUENCY : 1000 HZ

ESTIMATION OF VO

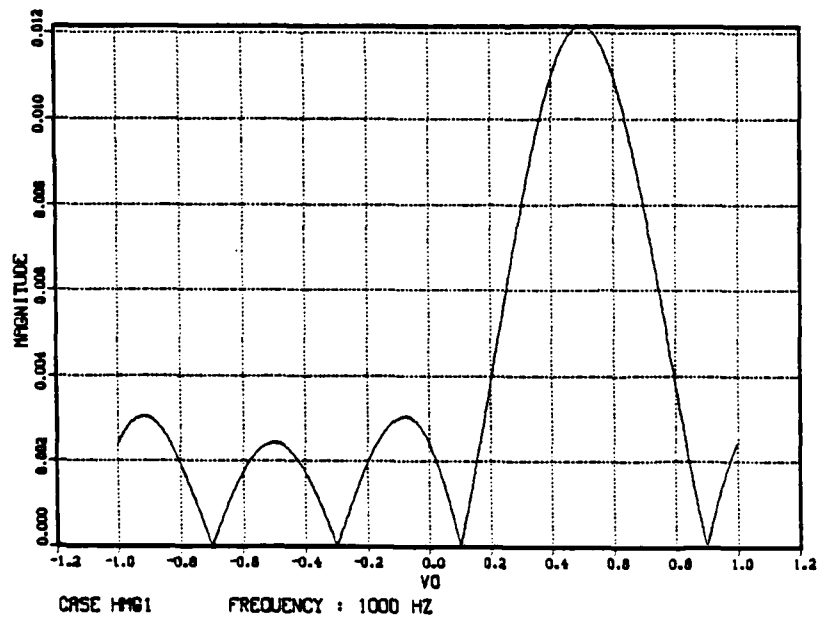CASE HMG1   FREQUENCY : 1000 HZ
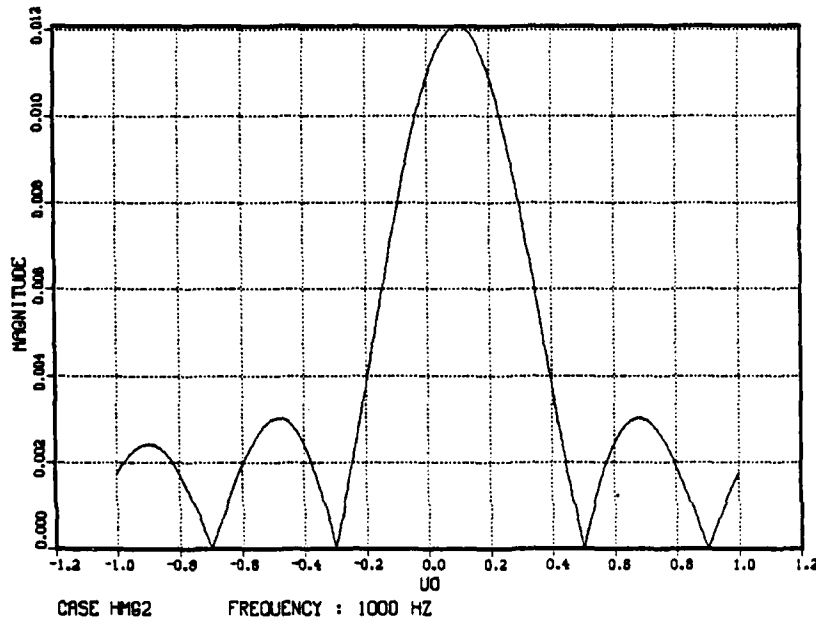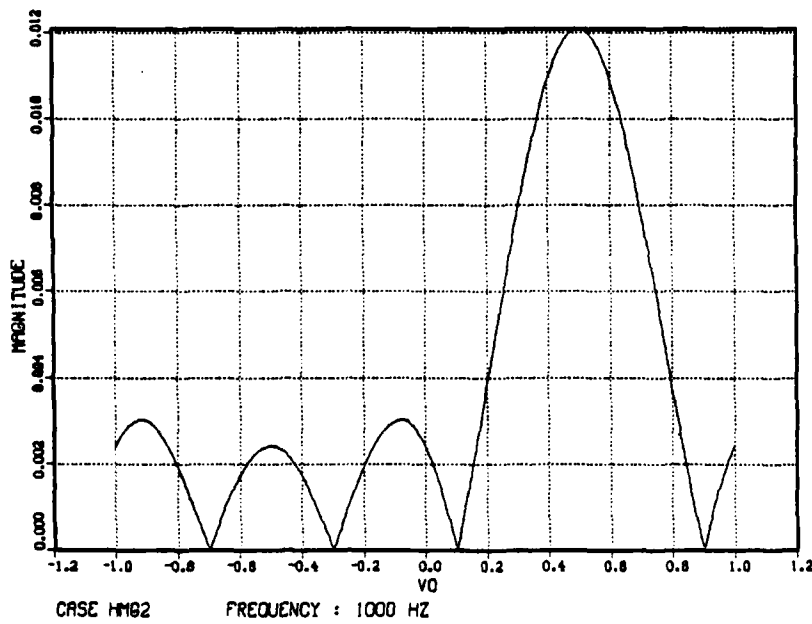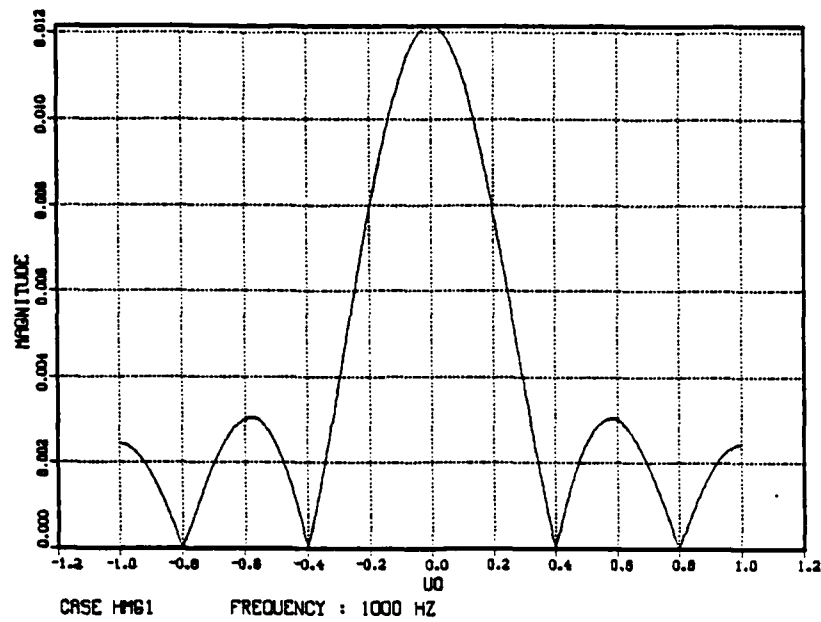
Fig. 7   Estimation of Direction of Propagation
          for Case HMG1

75

TABLE IV.10

Estimation of Fourier Series Coefficients
$Y_{SN}(q,0,0)$ for HMG8, INHMG8 and RINHMG8

Frequency (in Hz)	HMG8	INHMG8	RINHMG8
1000	0.0010987	0.0009705	0.0010341
2000	0.0098126	0.0098901	0.0102369
3000	0.0209366	0.0201906	0.0177316
4000	0.0138747	0.0122052	0.0087726
5000	0.0024539	0.0033176	0.0051316

Note: The Fourier series coefficients of the transmitted electrical signal are $c_k = a_k = 1$; $k = 1,2,\ldots,5$

TABLE IV.11

Estimated Values of $\hat{u}_o$, $\hat{v}_o$, $\hat{\theta}_o$ and $\hat{\psi}_o$

Case	Frequency (in Hz)	$\hat{u}_o$	$\hat{v}_o$	$\hat{\theta}_o$ (in degrees)	$\hat{\psi}_o$ (in degrees)
HMG8	1000	0.10	0.50	+31	+79
"	2000	0.10	0.50	+31	+79
"	3000	0.10	0.50	+31	+79
"	4000	0.10	0.50	+31	+79
"	5000	0.10	0.50	+31	+79
INHMG8	1000	0.10	0.49	+30	+78
"	2000	0.10	0.49	+30	+78
"	3000	0.10	0.49	+30	+78
"	4000	0.10	0.49	+30	+78
"	5000	0.10	0.49	+30	+78
RINHMG8	1000	0.10	0.63	+40	+81
"	2000	0.10	0.49	+30	+78
"	3000	0.10	0.53	+33	+79
"	4000	0.10	0.52	+32	+79
"	5000	0.10	-0.43	-26	-77

TABLE IV.9

Estimated Values $\hat{u}_o$, $\hat{v}_o$, $\hat{\theta}_o$ and $\hat{\psi}_o$

Case	$\hat{u}_o$	$\hat{v}_o$	$\hat{\theta}_o$ (in degrees)	$\hat{\psi}_o$ (in degrees)	
HMG1	0.000	0.500	+30.00	+90.00	
HMG2	0.100	0.500	+30.65	+78.69	
INHMG1	0.000	0.492	+29.47	+90.00	
INHMG2	0.101	0.492	+30.15	+78.40	
RINHMG2	0.101	0.523	+32.19	+79.07	(seed #1)
RINHMG1	0.000	0.523	+31.53	+90.00	(seed #1)
RINHMG1	0.000	0.508	+30.53	+90.00	(seed #2)

1) The line of sight angles from receive to transmit array (or target angles) are:

   HMG1, INHMG1, RINHMG1: $\theta_r = +30.00°$, $\psi_r = +90.00°$

   HMG2, INHMG2, RINHMG2: $\theta_r = +30.65°$, $\psi_r = +78.69°$

2) Note that equation (4.14) which is used to calculate estimates of target bearing angle from estimates of u_o and v_o returns two results. This is due to the ambiguity of a planar array. For the above table the appropriate values were selected.

73

TABLE IV.7

Magnitude of $Y_{SN}(q,m,s)$ Vs. Direction Cosine v for HMG1, HMG2

Direction Cosine v	HMG1	HMG2
0.484	.0121367	.0120534
0.489	.0121531	.0120696
0.494	.0121636	.0120800
0.499	.0121681	.0120844
0.504	.0121666	.0120828
0.509	.0121591	.0120754
0.514	.0121457	.0120620

TABLE IV.8

Magnitude of $Y_{SN}(q,m,s)$ Vs. Direction Cosine v for INHMG1, INHMG2

Direction Cosine v	INHMG1	INHMG2
0.475	.0116731	.0115947
0.480	.0116893	.0116111
0.485	.0117001	.0116215
0.490	.0117051	.0116264
0.495	.0117045	.0116258
0.500	.0116983	.0116196
0.505	.0116864	.0126078

TABLE IV.5

Magnitude of $Y_{SN}(q,r,n)$ Vs. Direction
Cosine u for HMG1, INHMG1

Direction Cosine u	HMG1	INHMG1
-0.015	.0121416	.0116804
-0.010	.0121566	.0116945
-0.005	.0121655	.0117030
0.0	.0121685	.0117058
0.005	.0121655	.0117030
0.010	.0121566	.0116945
0.015	.0121416	.0116804

TABLE IV.6

Magnitude of $Y_{SN}(q,r,n)$ Vs. Direction
Cosine u for HMG2, INHMG2

Direction Cosine u	HMG2	INHMG2
0.085	.0120593	.0116000
0.090	.0120744	.0116147
0.095	.0120836	.0116239
0.100	.0120869	.0116274
0.105	.0120842	.0116254
0.110	.0120756	.0116178
0.115	.0120611	.0116046

TABLE IV.3

Magnitude of Frequency Response Comparing Cases
Which Are Different Only in Frequency

Case	Frequency (in Hz)	$|H(f,0,0)|$
HMG1	1000	0.02434
HMG5	2000	0.03441
HMG7	4000	0.04866

TABLE IV.4

Magnitude of Frequency Response Comparing
Homogeneous and Inhomogeneous Cases

Case	$|H(f,0,0)|$
HMG1 - INHMG1	0.02434 - 0.02341
HMG2 - INHMG2	0.02417 - 0.02326
HMG5 - INHMG5	0.03441 - 0.03310

TABLE IV.1

Magnitude of Frequency Response Comparing Cases
Which Are Different Only in Total Range

| Case	Total Range (in m)	$\lvert H(f,0,0)\rvert$
HMG1	2000	0.02434
HMG3	1000	0.04868
HMG4	3000	0.01622

TABLE IV.2

Magnitude of Frequency Response Comparing Cases
Which Are Different Only in Cross Range

Case	Total Range (in m)	Cross Range (in m)	$\lvert H(f,0,0)\rvert$
HMG1	2000	0.0	0.02434
HMG2	2000	200.0	0.02417
HMG6	2000	1224.75	0.01654

Estimation of v_o returns a slightly different value from the line of sight value for direction cosine v_r due to the inhomogeneous behavior of the medium. Figures 14, 15 and 16 demonstrate the increasing directivity of the receive array with increasing frequency, thus leading to more accurate estimates for higher frequencies.

Figures 17, 18 and 19 clearly show the strong influence of the randomness on the resulting angular spectrum. The randomness creates strong "false" sidelobes and causes an offset of the estimated value of direction cosine v_o. The effects of the randomness increase with increasing frequency. At $f = 5000$ Hz (Fig. 19) the estimate of v_o is determined by a spurious side lobe and returns a totally wrong value. Table IV.11 shows estimated values of u_o and v_o at the different frequencies and their associated estimates of target elevation and bearing angles, $\hat{\theta}_o$ and $\hat{\psi}_o$, respectively.
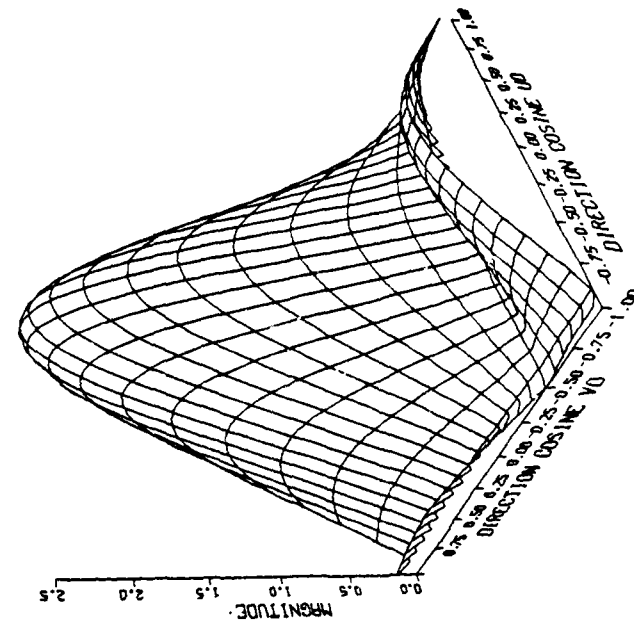
f = 2000 Hz
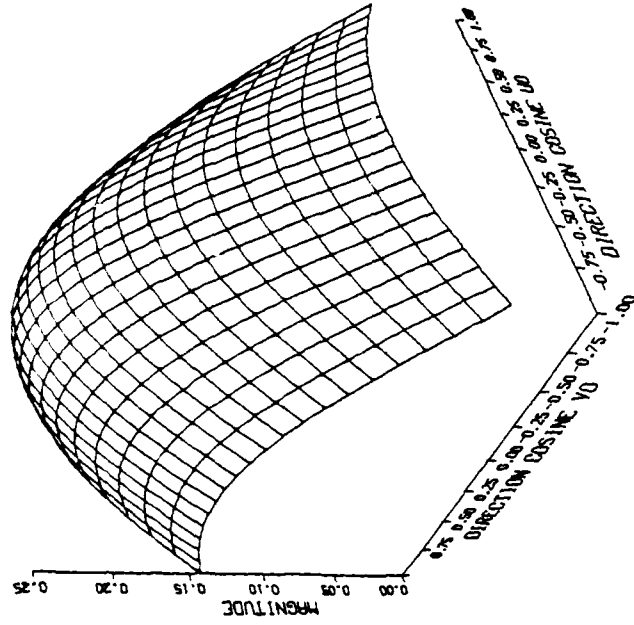
f = 1000 Hz

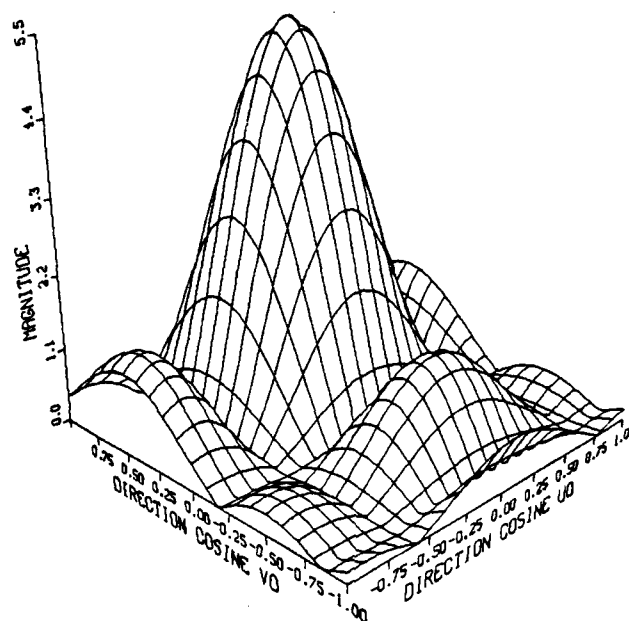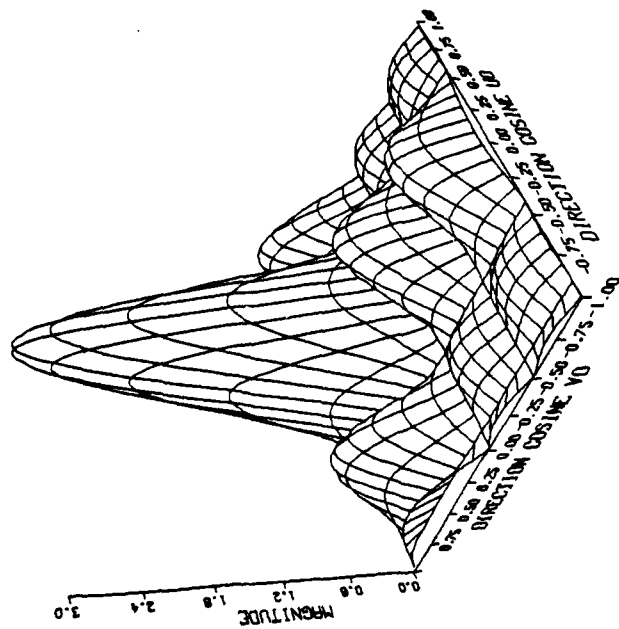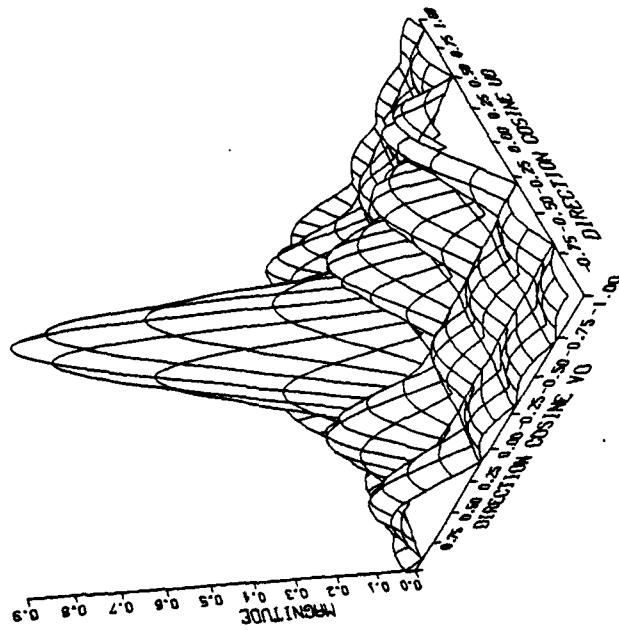Fig. 14 Angular Spectrum for Case INHMG8
at f = 1000 and f = 2000 Hz

82

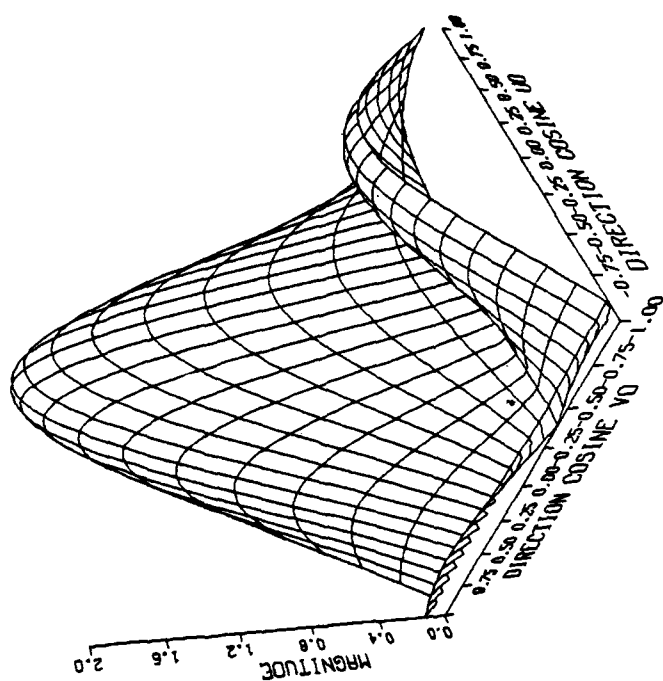Fig. 15   Angular Spectrum for Case
           INHMG8 at f = 3000 Hz

f = 4000 Hz
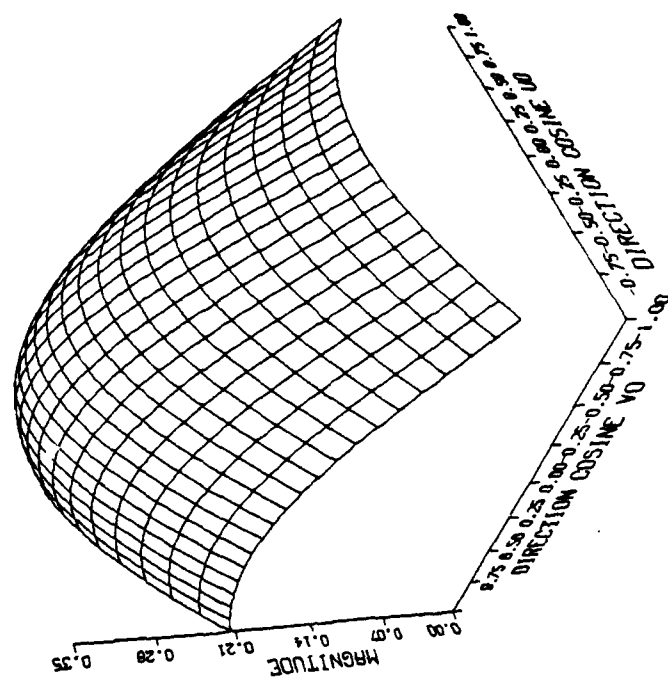
f = 5000 Hz

Fig. 16 Angular Spectrum for Case INHMG8 at f = 4000 and f = 5000 Hz

f = 1000 Hz   f = 2000 Hz

Fig. 17 Angular Spectrum for Case RINHMG8 at f = 1000 and f = 2000 Hz
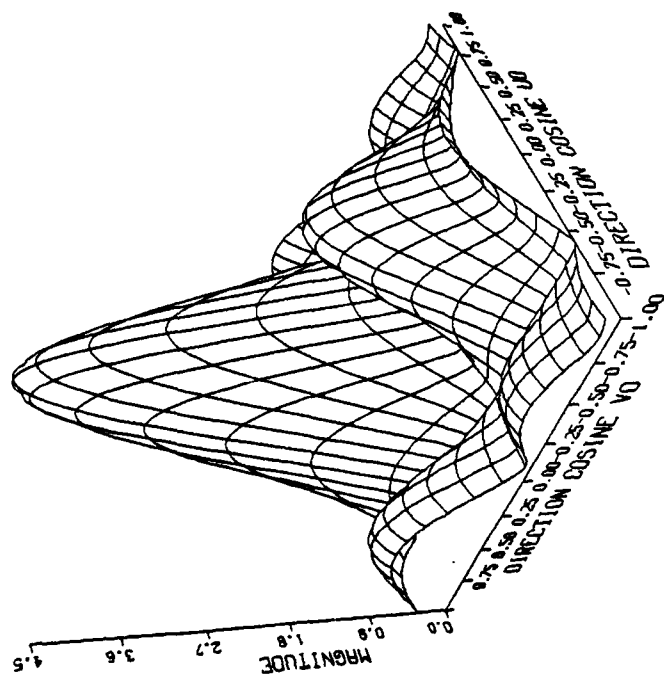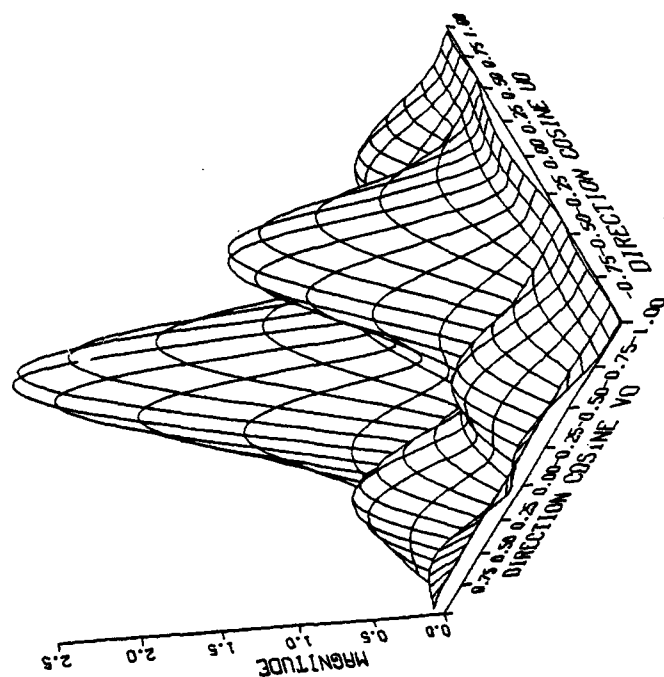
f = 3000 Hz   f = 4000 Hz

Fig. 18 Angular Spectrum for Case RINHMG8 at f = 3000 and f = 4000 Hz

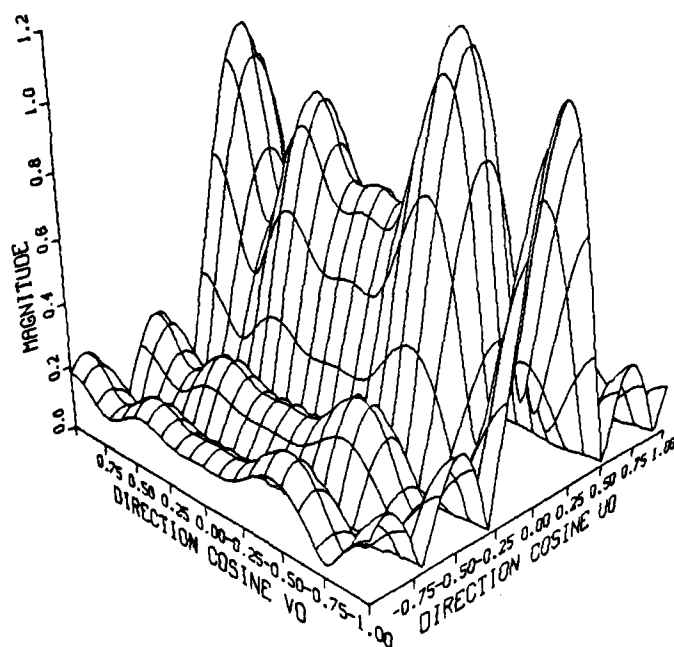Fig. 19   Angular Spectrum for Case
          RINHMG8 at f = 5000 Hz

V. CONCLUSIONS AND RECOMMENDATIONS

Computer simulation of a mathematical model of wave propagation through a random, space-variant, time-invariant, ocean medium between two planar arrays has been accomplished. The computer simulation incorporates an index of refraction which is only a function of depth. The deterministic component of the index of refraction represents a sound speed profile with constant gradient. The random component is assumed to have statistical properties independent of depth. The effects of the randomness on the electrical output signals at the different receiver elements are assumed to be uncorrelated.

The computer program was written in FORTRAN. It implements both analytical and numerical integration techniques. The results from both techniques are in close agreement.

A number of test cases have been run. Interpretation of the data for simple cases show results which are consistent with expectations from theory. The model correctly demonstrated the influences of the far field beam pattern of the transmit array, the source-receiver geometry, and the deterministic inhomogeneous behavior of the medium. Also, a random inhomogeneous medium was shown to affect the wave propagation and distort the frequency and angular spectra, leading to errors in the estimation of the Fourier series coefficients, target bearing angle, and target elevation angle. A final test case RINHMG8, with a transmit signal containing several frequency

components demonstrated a complex dependence on the above
mentioned factors, making interpretation of the results diffi-
cult. The effect of the randomness was very pronounced in
this case.

The computer program could be further improved by imple-
menting a more sophisticated method to simulate the randomness
of the medium. The assumption that the random phase terms at
the different receiver elements are uncorrelated breaks down
for small interelement spacings. The computer program can
also be easily modified to accommodate a more complex sound
speed profile in which the gradient is a function of depth,
for example.

. Future application of the model could be devoted to
investigating the propagation of more complex transmit signals.
One could also investigate the effects of the randomness of
the ocean medium on signal processing using different sizes
of receive arrays, i.e., increasing the number of elements.

LIST OF REFERENCES

1. Ziomek, L.J., _Underwater Acoustics--A Linear System Theory Approach_, Academic Press, Orlando, Florida (unpublished).

2. Ibid., Chapter 7, Section 7.2.1.

3. Ibid., Chapter 7, Section 7.2.2.

4. Ibid., Chapter 5, Section 5.1.

5. Laval, R., "Sound Propagation Effects on Signal Processing," _Signal Processing_, edited by Griffiths, P.L. and others, pp. 223-241, Academic Press, New York, 1973.

6. Laval, R., "Time-Frequency-Space Generalized Coherence and Scattering Functions," _Aspects of Signal Processing_, edited by Tacconi, G., Vol. I, pp. 69-87, D. Reidel Publishing Company, Dordrecht, The Netherlands, 1977.

7. Laval, R. and Labasque, Y., "Medium Inhomogeneities and Instabilities: Effects on Spatial and Temporal Processing," _Underwater Acoustics and Signal Processing_, edited by Bjorno, L., pp. 41-70, D. Reidel Publishing Company, Dordrecht, The Netherlands, 1981.

8. Middleton, D., "A Statistical Theory of Reverberation and Similar First-Order Scattered Fields. Part III: Waveforms and Fields," _IEEE Trans. Information Theory_, Vol. 18, pp. 35-67, 1972.

9. Middleton, D., "The Underwater Medium as a Generalized Communication Channel," _Underwater Acoustics and Signal Processing_, edited by Bjorno, L., pp. 589-612, D. Reidel Publishing Company, Dordrecht, The Netherlands, 1981.

10. Officer, C.B., _Introduction to the Theory of Sound Transmission_, pp. 67-68, McGraw-Hill, New York, 1958.

11. Gerald, C.T., _Applied Numerical Analysis_, pp. 60-72, Addison-Wesley, 1970.

12. Moursund, D.G. and Duris, C.S., _Elementary Theory and Application of Numerical Analysis_, pp. 194-199, McGraw-Hill, 1967.

13. Squire, W., _Integration for Engineers and Scientists_, American Elsevier Publishing Company, New York, 1970.

14. Brekhovskikh, L.M., *Waves in Layered Media*, pp. 234-239,
    Academic Press, New York, 1980.

15. Brekhovskikh, L. and Lysanov, Yu., *Fundamentals of Ocean
    Acoustics*, p. 3, Springer-Verlag, 1982.

16. Clarke, R.H., "Sound Propagation in a Variable Ocean,"
    Journal of Sound and Vibration, Vol. 34, p. 472, 1974.

17. Mintzer, D., "Wave Propagation in a Randomly Inhomogeneous
    Medium I," *Journal of the Acoustic Society of America*,
    Vol. 25, p. 925, 1953.

18. Mintzer, D., "Wave Propagation in a Randomly Inhomogeneous
    Medium I and II," *Journal of the Acoustic Society of
    America*, Vol. 26, p. 1110, 1953.

19. Kinsler, L.E., and others, *Fundamentals of Acoustics*,
    p. 401, 3rd ed., Wiley & Sons, 1981.

INITIAL DISTRIBUTION LIST

No. Copies

1. Defense Technical Information Center   2
   Cameron Station
   Alexandria, Virginia   22314

2. Library, Code 0142   2
   Naval Postgraduate School
   Monterey, California   93943

3. Department Library, Code 61   1
   Department of Physics
   Naval Postgraduate School
   Monterey, California   93943

4. Assistant Professor L.J. Ziomek, Code 62Zm   15
   Department of Electrical and
     Computer Engineering
   Naval Postgraduate School
   Monterey, California   93943

5. Inspecteur Onderwijs Zeemacht   2
   Ministry of Defense (Navy)
   Koningin Marialaan 17
   Den Haag
   The Netherlands

6. Vlagofficier belast met de officiersvorming 2
   Koninklijk instituut voor de Marine
   Het Nieuwe Diep 8
   Den Helder
   The Netherlands

7. LT J. Vos   3
   p/a Dorpsstraat 12
   Schipluiden, 2636 CC
   The Netherlands

8. Mr. Charles Stewart   1
   DARPA
   1400 Wilson Blvd.
   Arlington, VA   22200

END

FILMED

6-85

DTIC